ESTABLISHMENT OF THE PYRUVATE DEHYDROGENASE COMPLEX AS A CENTRAL REGULATOR OF MITOCHONDRIAL REDOX WITHIN SKELETAL MUSCLE

by

Kelsey H. Fisher-Wellman

April 26, 2013

Director of Dissertation: P. Darrell Neufer

Department of Kinesiology

Once regarded as “byproducts” of aerobic metabolism, the production of superoxide/H_2O_2 is now understood to be a highly specialized and extensively regulated process responsible for exerting control over a vast number of thiol-containing proteins, collectively referred to as the redox-sensitive proteome. Although disruptions within this process, secondary to elevated peroxide exposure, have been linked to disease, delineation of the sources and mechanisms regulating this increased peroxide burden remain poorly defined and as such difficult to target using pharmacotherapy. Herein we demonstrate a role for pyruvate dehydrogenase (PDH) as a key source of H_2O_2 under physiological constraints in which respiratory chain-dependent electron leak is negligible. PDH is shown to generate H_2O_2 as a function of glutathione content, matrix metabolic balance, as well as antioxidant reductase activity. With respect to the latter, manipulation of matrix redox buffering reveals a novel mechanism whereby H_2O_2 producing NADH-linked dehydrogenases, such as PDH, are functionally linked to the

redox buffering network within skeletal muscle through the activity of nicotinamide nucleotide transhydrogenase (NNT). These findings highlight the importance of NNT and the entire redox buffering system in regulating cytosolic peroxide emission and suggest a novel and pivotal role for PDH as a redox-sensitive reporter of matrix redox buffering integrity and nutrient status.

ESTABLISHMENT OF THE PYRUVATE DEHYDROGENASE COMPLEX AS A CENTRAL REGULATOR OF MITOCHONDRIAL REDOX WITHIN SKELETAL MUSCLE

A Dissertation

Presented To the Faculty of the Department of Kinesiology

East Carolina University

In Partial Fulfillment of the Requirements for the Degree

Doctor of Philosophy

by

Kelsey H. Fisher-Wellman

April 26, 2013

Establishment of the pyruvate dehydrogenase complex as a central regulator of mitochondrial redox within skeletal muscle

Establishment of the pyruvate dehydrogenase complex as a central regulator of mitochondrial redox within skeletal muscle

by

Kelsey H. Fisher-Wellman

APPROVED BY:

DISSERTATION ADVISOR:_____

P. Darrell Neufer, Ph.D.

COMMITTEE MEMBER:

_____

David A. Brown, Ph.D.

COMMITTEE MEMBER:

_____

David A. Tulis, PhD

COMMITTEE MEMBER:

_____

Donghai Zheng, PhD

COMMITTEE MEMBER:

_____

Jeffrey Brault, PhD

CHAIR OF THE DEPARTMENT OF KINESIOLOGY

_____

Stacey R. Altman, PhD

DEAN OF THE GRADUATE SCHOOL

_____

Paul J. Gemperline, PhD

ACKNOWLEDGEMENTS

The completion of this work would not have been possible without the support of many individuals. First and foremost I would like to express my most sincere gratitude to my mentor Dr. P. Darrell Neufer for the opportunity to pursue my doctorate degree in his lab. I have tremendous respect and admiration for Dr. Neufer both as a person and as a scientist and working in his lab over the past four years has been one the most rewarding experiences of my life. I would also like to thank my colleagues within Dr. Neufer's lab for their expert guidance, technical assistance and overall support of my research projects over the last several years. Lastly, I would like to thank my committee members, Drs. David Brown, David Tulis, Jeff Brault, and Donghai Zheng for their support and continued guidance throughout the dissertation process. The atmosphere created by these individuals, as well as by the entire faculty and staff within the Human Performance Laboratory and Departments of Kinesiology and Physiology at the Brody School of Medicine has always been one of cooperation and support, two characteristics which make East Carolina University an ideal place to pursue a doctoral degree.

TABLE OF CONTENTS

LIST OF FIGURES

LIST OF SYMBOLS AND ABBREVIATIONS

6J	C57BL/6J mice
6N	C57BL/6N mice
^{3}H-2-DOG	^{3}H-2-deoxyglucose
ADP	Adenosine diphosphate
AF	Auranofin
ANOVA	Analysis of variance
ANT	Adenine nucleotide translocase
ATP	Adenosine triphosphate
AU	Arbitrary units
AUC	Area under curve
BCNU	Bis-chloroethylnitrosourea
CDNB	1-chloro-2,4-dinitrobenzene
CoA	Coenzyme A
Complex I	NADH:ubiquinone oxidoreductase
Complex II	Succinate dehydrogenase
Complex III	Coenzyme Q : cytochrome c — oxidoreductase
Complex IV	Cytochrome c oxidase
Complex V	Mitochondrial ATP synthase
COX-IV	Cytochrome C oxidase, isoform IV
CrAT	Carnitine acetyltransferase
Cys	Cysteine
Cyto C	Cytochrome C
DHLA	Reduced dihydrolipoate

DMSO	Dimethyl sulfoxide
DNA	Deoxyribonucleic acid
DPI	Diphenyliodonium chloride
DTT	Dithiothreitol, a strong chemical reductant
E1	Pyruvate dehydrogenase subunit of the PDH complex
E2	Dihydrolipoyl transacetylase subunit of the PDH complex
E3	Dihydrolipoyl dehydrogenase subunit of the PDH complex
EDL	Extensor digitorum longus muscle, mostly fast-twitch fibers
EDTA	Ethylenediaminetetraacetic acid,
EGTA	Ethylene-bis(oxyethylenenitrilo)tetraacetic acid
ETF	Electron transfer flavoprotein
ETS	Mitochondrial electron transport system
$FADH_2$	Flavin adenine dinucleotide
FCCP	Carbonylcyanide-p-trifluoromethoxyphenylhydrazone
FMN	Flavin mononucleotide
G	Glutamate
G3P	Glycerol-3-phosphate
GSH	Reduced glutathione
GSSG	Oxidized glutathione
H_2O_2	Hydrogen peroxide
HEPES	4-(2-hydroxyethyl)-1-piperazineethanesulfonic acid
HFD	High fat diet
HRP	Horseradish peroxidase
IDH	NADP-linked isocitrate dehydrogenase

IPGTT	Intraperitoneal glucose tolerance test
IR	Insulin resistance
JH_2O_2	Mitochondrial H_2O_2 emission/production rate
*J*NADH	NADH production rate
JO_2	Mitochondrial oxygen consumption rate
kDa,	Kilodalton
KHB	Krebs-Henseleit buffer
LA	Oxidized lipoate
M	Malate
NADH	Reduced nicotinamide adenine dinucleotide
NEM	N-ethylmaleimide
NNT	Nicotinamide nucleotide transhydrogenase
$O2^{-}$•	Superoxide anion
O2K	Oroboros oxygraph-2 k
OAC	Oxaloacetate
OXPHOS	Oxidative phosphorylation
PC	Palmitoyl-L-carnitine
PDH	Pyruvate dehydrogenase
PDK4	Pyruvate dehydrogenase kinase isoenzyme 4
PVDF	Polyvinylidene fluoride
Pyr	Pyruvate
RG	Red gastrocnemius
ROS	Reactive oxygen species
RS-	Thiolate anions

S	Succinate
-S-	Thioether
S.E.M.	Standard error mean
SD	Sprague-Dawley rat
SDS	Sodium dodecyl sulfate
SDS-PAGE	Sodium dodecyl sulfate polyacrylamide gel electrophoresis
-SH	Thiol
$-SO^{-}$	Sulfenate
$-SO_2^{-}$	Sulfinate
$-SO_2H$	Sulfinic acid
$-SO_3^{-}$	Sulfonate
$-SO_3H$	Sulfonic acid
SOD	Superoxide dismutase
-SOH	Sulfenic acid
State I	Respiration supported by mitochondria alone
State II	Respiration supported by ADP alone
State III	Respiration supported by substrates and ADP
State IV	Non-phosphorylating respiration
TCA cycle	Tricarboxylic acid cycle
TPP^{+}	Tetraphenylphosphonium cation
Δp	Mitochondrial proton electrochemical gradient (proton motive force)
$\Delta\Psi$	Mitochondrial membrane potential

CHAPTER 1: REVIEW OF THE LITERATURE

Portions of Chapter I adapted from: **Fisher-Wellman KH**, Neufer PD. Linking mitochondrial bioenergetics to insulin resistance via redox biology. Trends Endocrinol Metab. 2012 Mar;23(3):142-53. (PMID: 22305519)

Organization and function of the respiratory system

In 1961, Peter Mitchell published a unique hypothesis regarding cellular bioenergetic conservation (39), for which he was awarded the Nobel Prize in chemistry in 1978. Termed the "chemiosmotic theory of oxidative phosphorylation" (also known as chemiosmosis), at its core is the notion of coupling hydrogen and electron transfer through an energy-conserving membrane to the phosphorylation of ADP to form ATP. The mitochondrial electron transport system consists of several multi-polypeptide protein complexes (I-V) embedded in the inner mitochondrial membrane that receive electrons from reducing equivalents (i.e., NADH, $FADH_2$) generated by dehydrogenases (e.g., pyruvate dehydrogenase, α-ketoglutarate dehydrogenase, acyl-CoA dehydrogenase, etc). These electrons are transferred through a series of electron carriers in the respiratory chain with O_2 serving as the final electron acceptor, ultimately reducing $½O_2$ to H_2O. Each of the electron carriers represents a redox couple (i.e., species capable of existing in a reduced or oxidized state) with a characteristic *reduction potential* – a measure of the tendency of the oxidized species to accept an electron(s). A negative reduction potential indicates the reduced species has a high tendency to donate (lose) an electron(s) (e.g., NADH) and a positive reduction potential indicates the oxidized species has a high tendency to accept (gain) an electron(s) (e.g., O_2). The electron carriers in the respiratory chain are ordered in such a way that the

reduction potentials progressively increase (i.e., become more positive) from one redox couple to another. In three of these complexes (I, III and IV), the difference in reduction potential (i.e., release of energy) across successive redox couples is sufficient to drive the translocation of protons from the matrix to the inner membrane space. This creates a proton gradient across the inner membrane that is derived from both the concentration (ΔpH) and the electrical potential ($\Delta\tilde{u}_H^+$) difference across the membrane. By bioenergetic convention, $\Delta\tilde{u}_H^+$ is converted to units of electrical potential (i.e., mV), and commonly referred to as the membrane potential ($\Delta\Psi$). Although ΔpH and $\Delta\Psi$ together comprise the total proton motive force (Δp), $\Delta\Psi$ is by far the dominant component and often used synonymously with Δp. The essence of the chemiosmotic theory is that the electrical-chemical potential energy created by the generation of Δp is sufficient to drive the synthesis of ATP as protons flow back through the ATP synthase complex into the matrix.

Several features of the respiratory system, some counterintuitive, are essential to understanding how cellular energy balance is normally governed and therefore how cellular energy surplus may affect the system. First, similar to an electrical circuit, the transport of electrons through the respiratory chain is an inherent property of the system – it occurs automatically. Second, for the most part, electron flow and proton pumping are tightly coupled; that is, one does not occur without the other. The third feature requires visualizing the boundaries that govern the system in real time. Consider starting with a de-energized system. To activate respiration, fuel (i.e., NADH, $FADH_2$) is added which automatically initiates electron flow, proton pumping, and O_2 consumption. However, as $\Delta\Psi$ begins to build on the outer surface of the inner membrane, a “back

pressure" is created which begins to oppose the pumping of protons, thereby gradually slowing electron flow and O_2 consumption. Eventually the point is reached at which the force driving the pumping of protons out of the matrix (i.e., the *reduction potential* span from the NAD^+/NADH couple to the $O_2/2H_2O$ couple) is completely counter-balanced by the high $\Delta\Psi$. This creates "static head" equilibrium. Fortunately, mitochondria never reach this state (i.e., we never stop consuming O_2) because the mitochondrial inner membrane is inherently leaky to protons. This basal rate of proton conductance ensures that $\Delta\Psi$ is at some value less than maximum, thereby "allowing" electron flow, proton pumping, and O_2 consumption to operate at an "idling" rate (known as *state 2 respiration*). If another avenue for protons to flow back into the matrix is created (e.g., via ATP synthase catalyzing re-phosphorylation of ADP), then the back pressure ($\Delta\Psi$) is further reduced and electron flow, proton pumping, and oxygen consumption increase accordingly (known as *state 3 respiration*). Once all of the ATP is resynthesized, the system slows back to the idling rate (known as *state 4 respiration*) The critical point is that the mitochondrial respiratory system is a "primed engine", automatically adjusting to each change in the rate of proton re-entry into the matrix with a corresponding change in electron flow and O_2 consumption. The fourth and final feature should be apparent from the first three; the rate at which the respiratory system operates is governed by energy demand ("pull"), not energy supply ("push"). Proton conductance (via leak and ATP synthase) dictates the rate of electron flow and therefore the demand for reducing equivalents (e.g., NADH and $FADH_2$) which, in turn, regulates the rate of substrate uptake and flux through catabolic pathways.

How then may an excess of metabolic fuel affect the system? To address this question requires consideration of *redox state,* which is defined as the product of the *reduction potential* and the *reducing capacity* (i.e., the concentration of the reduced species) of a *redox couple*. The higher the concentration of the reduced species, the more reduced or "charged" the redox state. Thus, a provision of excess reducing equivalents due to over nutrition will increase the "pressure head" at the entry point of electrons into complex I (↑ $NADH/NAD^+$) and/or the Q pool (↑ $FADH_2/FAD^+$), in either case elevating the redox state and membrane potential of the respiratory system. Several of the redox couples within the electron transport chain transfer single rather than two electrons and are therefore susceptible to leaking electrons directly to surrounding O_2 to form the free-radical superoxide ($O_2\bullet^-$). Under state 3 conditions, the redox state of the system is below the threshold at which electrons will leak to O_2. However, at or near state 4 respiration, the respiratory system is in its most reduced state such that the rate at which $O_2\bullet^-$ is produced is extremely sensitive to the redox state of the system, increasing exponentially with even small increases in membrane potential (34, 37, 38). Fortunately, $O_2\bullet^-$ is rapidly converted by manganese superoxide dismutase (MnSOD) to the two-electron non-radical hydrogen peroxide (H_2O_2). H_2O_2 in turn can be further reduced to H_2O in the mitochondrial matrix by glutathione (GSH) or the thioredoxin/peroxiredoxin systems, or can freely diffuses out of the mitochondria where it again is buffered by GSH. Thus in a resting cell, the mitochondrial respiratory system functions as a redox pressure gauge that senses and reflects cellular metabolic balance. When in positive balance, electron leak serves as a release valve, accelerating mitochondrial $O_2\bullet^-$ production and H_2O_2 emission.

Sites of electron leak within mammalian mitochondria

Currently identified sites of electron leak within the respiratory chain include the flavin mononucleotide (site IF) and ubiquinone binding site (site IQ) within complex I, the quinone at centre “o” within complex III (site IIIQo), the quinone binding site within glycerol-3-phosphate dehydrogenase (G3PDC), and electron transferring flavoprotein Q oxioreductase (ETFQOR) (6) (**Figure 1**). Additional non-respiratory chain sites include the matrix dehydrogenase enzyme complexes pyruvate dehydrogenase (PDH) and α-ketoglutarate dehydrogenase (KGDH), both of which are believed to generate $O_2\bullet^-$ via interactions between the dihydrolipoyl transacetylase (E2) and the FAD-containing dihydrolipoamide dehydrogenase (E3) components of their respective enzyme complexes (53). With respect to the former, mammalian PDH is comprised of three main catalytic components (E1-pyruvate dehydrogenase, E2, E3), which combine to form a large (~9.5 MDa) multi-subunit holoenzyme with a stoichiometry of 40:40:20 (E1:E2:E3) (7). Maximal PDH/KGDH-stimulated rates of $O_2\bullet^-$ are observed when the steady-state ratio of dihydrolipoate (DHLA) to lipoate (LA) within E2 is shifted in favor of the reduced form and supply of NAD^+ is decreased (i.e., ↑DHLA/LA, ↓NADH/NAD+). Under these conditions, it is believed that E3 catalyzes a $1e^-$ oxidation reaction between O_2 and E2-bound dihydrolipoate, in turn leading to either $O_2\bullet^-$ and/or a thiyl radical (8, 9).

Linking mitochondrial bioenergetics to protein function via redox biology

The production of $O_2\bullet^-/H_2O_2$ within biological systems was originally thought to exist merely as a deleterious byproduct of aerobic metabolism, that under normal (i.e., healthy) conditions were readily scavenged/degraded by the elaborate antioxidant

defense machinery. At any one time point, the actual oxidative burden imposed to the system was believed to be dictated by the net balance of these two opposing systems (H_2O_2 production vs. antioxidant buffering). In line with this notion, the term oxidative stress is commonly utilized as a general term to indicate any biological situation in which the production of H_2O_2 exceeds the ameliorating capabilities of the antioxidant defense system, potentially resulting in modification/ damage to various macromolecules (18). This oxidative damage has been suggested to play a role in the etiology of a myriad of human diseases, as well as the aging process (12). Although, the preponderance of evidence certainly suggests a critical role for these species in ill health/disease, specific cause and effect mechanisms have proven difficult to establish. Moreover, the use of various antioxidant treatments/interventions in an attempt to curtail disease progression and/or slow the aging process has been met with minimal success (12). If oxidative damage mediated by these species are indeed so critical in human pathophysiology, and operating under the belief that this damage occurs under conditions in which free radical expression exceeds that of defenses, why then would exogenous supply of antioxidants not be met with positive outcomes? One potential explanation lies in the continual observation that these prooxidant species are not merely byproducts that the system must constantly protect against.

H_2O_2 is now widely accepted as a critical signaling molecule within biological systems (14, 28). In fact, the continuous generation of H_2O_2, at concentrations far below those indicative of “oxidative stress”, is believed to be involved in the regulation of various redox signaling pathways, referred to as “redox circuits” (**Figure 2**) (28). Cellular redox circuits are analogous to electrical circuits in that they are established by

a set of linked oxidation/reduction reactions initiated by a difference in reduction potential between two redox couples (i.e., voltage) and propogated as electron flow (i.e., electrical current) among successive redox couples with higher reduction potentials. The glutathione (2GSH/GSSG) and thioredoxin (Trx_{Red}/Trx_{Ox}) redox couples, both of which are expressed at high levels and derive their reducing power from $NADPH/NADP^+$, serve as the common control nodes of the circuit (i.e., the wiring) and the direct link to cysteine (Cys) residues within specific redox-sensitive proteins. Electron flux through these couples is thought to be rapid and continuous reflecting the rates of reducing ($NADPH/NADP^+$, the "charge" within the circuit) and oxidizing (H_2O_2 production, the "dissipation of charge") inputs. Under normal circumstances, the balance strongly favors reduction of protein Cys and thus an overall reduced cellular redox environment. Of the ~214,000 Cys residues within the proteome, it is estimated >20,000 are redox sensitive (i.e., capable of oscillating between a reduced and oxidized state as a redox couple) (28). The activity/function of these redox sensitive proteins is dependent upon the redox state of the sulfur atoms within these Cys moieties, thus giving rise to the term "sulfur switches" (28). The sulfur atom within Cys can exist as a reduced thiol (-SH) or in a variety of oxidation states, including as a thiolate anion ($-S^-$), sulfenate ($-SO^-$), disulfide (-S-S) sulfinate ($-SO_2^-$), or sulfonate ($-SO_3^-$) (28). Each of these redox-sensitive switches has a characteristic reduction potential, or sensitivity to the redox circuit, that reflects in large part the degree to which each redox sensitive Cys within the protein is spatially and kinetically insulated from the circuit. Alterations in the redox state of these "sulfur switches" induces a variety of effects, including changes in protein conformation, enzyme activity, transporter activity, ligand-receptor binding,

protein-protein interaction, protein trafficking, protein degradation, and transcriptional binding to DNA (28).

Nicotinamide nucleotide transhydrogenase (NNT) as a principle source of reducing power

Much of the literature thus far has focused on the potential consequence of elevated peroxide production in terms of contributing to human disease. However; based on the current working model of the organization/structural characteristics of redox signaling networks, protein redox status is primarily dictated not by H_2O_2 production, but rater by supply of reducing power (i.e., NADPH). That is, alterations in cellular redox in the context of a redox-mediated signaling event could just as easily be propagated via a reduction in NADPH supply as they could by an increase in H_2O_2 production. This concept represents a potential paradigm shift within the field in which investigative emphasis is directed not only towards uncovering the specific proteins responsible for H_2O_2 generation, but also to those tasked with the maintenance of cellular reducing power (i.e., NADPH producing enzymes).

Cellular sources of NADPH include glucose-6-phosphate dehydrogenase and 6-phosphogluconate dehydrogenase within the pentose phosphate pathway, as well the mitochondrial enzymes NADP-linked isocitrate dehydrogenase, decarboxylating malate dehydrogenase (malic enzyme; also present in the cytosol) and nicotinamide nucleotide transhydrogenase (NNT) (46, 47). NNT is particularly interesting in that it is a proton-translocating enzyme that utilizes the electrochemical proton motive force (Δp) generated by the respiratory complexes to drive the thermodynamically unfavorable

reduction of $NADP^+$ from NADH (21). Approximately 50% of mitochondrial NADPH is eliminated in the presence of an uncoupler, thus suggesting a significant contribution of NNT to matrix NADPH supply (46). As expected, knockout of NNT in Caenorhabditis elegans (5), as well as PC12 cells (60) has indeed been shown to impair cellular redox homeostasis (oxidative shift in the glutathione pool), as well as increase sensitivity to peroxide exposure, and alter energy metabolism (reduced respiration and levels of ATP).

Role of NNT in controlling insulin secretion: Story of the C57BL/6J line

NNT gained considerable attention within the field of diabetes research when mutations within the NNT gene were successfully linked to the glucose intolerant phenotype of the C57BL/6J mouse strain (16, 57). C57BL/6J mice are one of the most routinely employed animal models of glucose intolerance, due primarily to their increased susceptibility to develop insulin resistance and overt type II diabetes when fed a high fat diet (HFD) (30, 55, 56). Interestingly, when fed a HFD, these mice are also characterized by an increase propensity for weight gain, despite similar levels of nutrient intake (54). In an elegant series of experiments conducted by Toye et al., (57) the phenotype C57BL/6J strain was mapped to a naturally occurring in-frame five exon deletion within the NNT gene, which removes exons 7-11 of the mature peptide, effectively creating an NNT whole body knockout (16, 23). This mutation is believed to have occurred sometime between 1970 and 1984 and is apparently specific to the pure C57BL/6J strain produced only by the Jackson Laboratory (http://jaxmice.jax.org/strain/000664.html). Follow up experiments in which functional NNT was reintroduced via transgenic expression successfully rescued the impaired

insulin secretion and glucose intolerant phenotype of the C57BL/6J mice. A role for NNT in controlling pancreatic insulin secretion was subsequently demonstrated using siRNA directed at NNT within an insulin secreting cell line (15). With regards to the mechanism of action, loss of NNT is believed to elevate "oxidative stress" within the beta cell in response to glucose, thereby lowering the ATP: ADP ratio and delaying closure of the K_{ATP} channel (15, 46). While much of the literature related to the C57BL/6J strain has focused on the impact of NNT on insulin secretion, very little is currently known about the effects of NNT loss on other tissues, specifically within insulin sensitive peripheral tissues such as skeletal muscle.

Central Hypothesis

The goal of this dissertation was to determine if the pyruvate dehydrogenase complex is a source of H_2O_2 production and therefore a component of the matrix redox network. The overriding hypothesis was that PDH and perhaps other NADH-linked dehydrogenases exist as continual sources of H_2O_2 necessary to establish various redox signaling networks within the matrix. In Chapter II we reveal PDH as a principle source of H_2O_2 within skeletal muscle under physiological constraints. In Chapter III, we demonstrate a role for NNT in controlling mitochondrial peroxide emission within skeletal muscle, as well as whole body energy metabolism. Under normal conditions, H_2O_2 generated by PDH was efficiently scavenged by the elaborate redox buffering systems present, all of which depend on continual NADPH generation for reducing power. However, loss of redox buffering integrity, either through depletions in cellular glutathione and/or NADPH supply, led to a dramatically accelerated rate of PDH-derived

H_2O_2 production, altering whole cell redox status and potentially contributing to disease. These data shed valuable insight related to the role of both PDH and NNT in controlling matrix redox status and whole body energy metabolism. Moreover, we hypothesize that the identified functional link between PDH-derived H_2O_2 production and NNT activity may have far reaching implications related to the glucose intolerant phenotype of the C57BL/6J strain, as well as the development of diet-induced insulin resistance.

Figure 1. Sites of electron leak within mammalian mitochondria. In mammalian mitochondria, currently identified sites of electron leak/superoxide formation in the electron transport system (ETS) include the flavin mononucleotide and ubiquinone binding site within complex I (I), the quinone at centre "o" within complex III (III), the quinone binding site within glycerol-3-phosphate dehydrogenase (G3PDH), and the electron transferring flavoprotein Q oxioreductase (ETF-QO). Additional non-respiratory system sources include the matrix soluble pyruvate (PDH) and alpha-ketoglutarate (KGDH) dehydrogenase complexes.

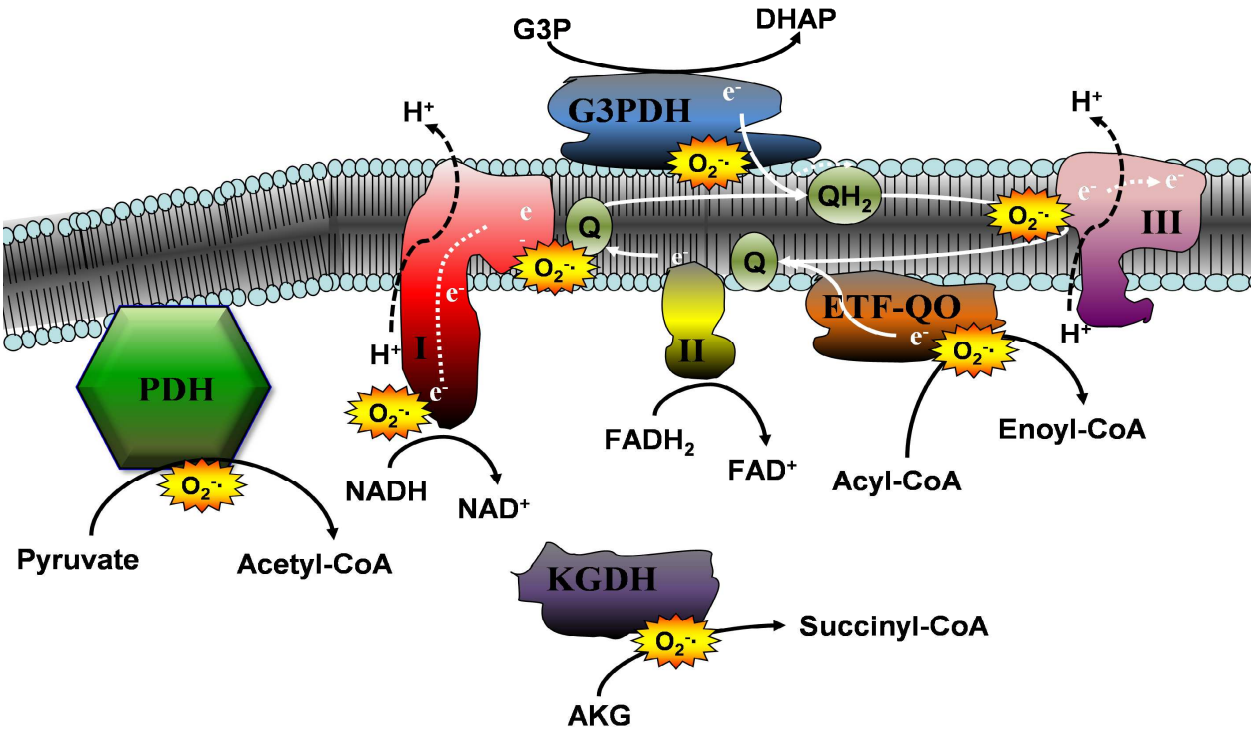

Figure 2. Simplified model of redox circuitry. Theoretical E_h values are shown in blue for the 2GSH/GSSG, Trx_{2SH}/Trx_{SS}, and NADPH/NADP+ redox couples, as well as their protein target. Electrons flow through the circuit from the NADPH/NADP+ couple to thiol (SH) moieties within exposed Cys. The overall driving force for reduction is determined by the mV differences in E_h between NADPH/NADP+ and the redox sensitive Cys-containing proteins (e.g., ΔE_h = -500 mV). The red text indicates the effects of a transient increase in mitochondrial H_2O_2 emission in the context of a redox mediated signaling event. Under these conditions, an oxidative shift in the redox environment (depicted as a positive shift in each couple's E_h), would reduce the overall driving force for the reduction of exposed Cys residues within the target protein (ΔE_h = -300 mV), thereby altering the redox state of the protein in favor of its oxidized form (e.g., either $2SO^-$ or SS) and leading to a cellular response. These responses are thought to function as a means of rheostat regulation rather than as a simple "on/off" mechanism. The blue/red bar on the left labeled "E" represents the intracellular redox environment. GR, glutathione reductase; TR, thioredoxin reductase; Gpx, glutathione peroxidase; Prx, peroxiredoxin.

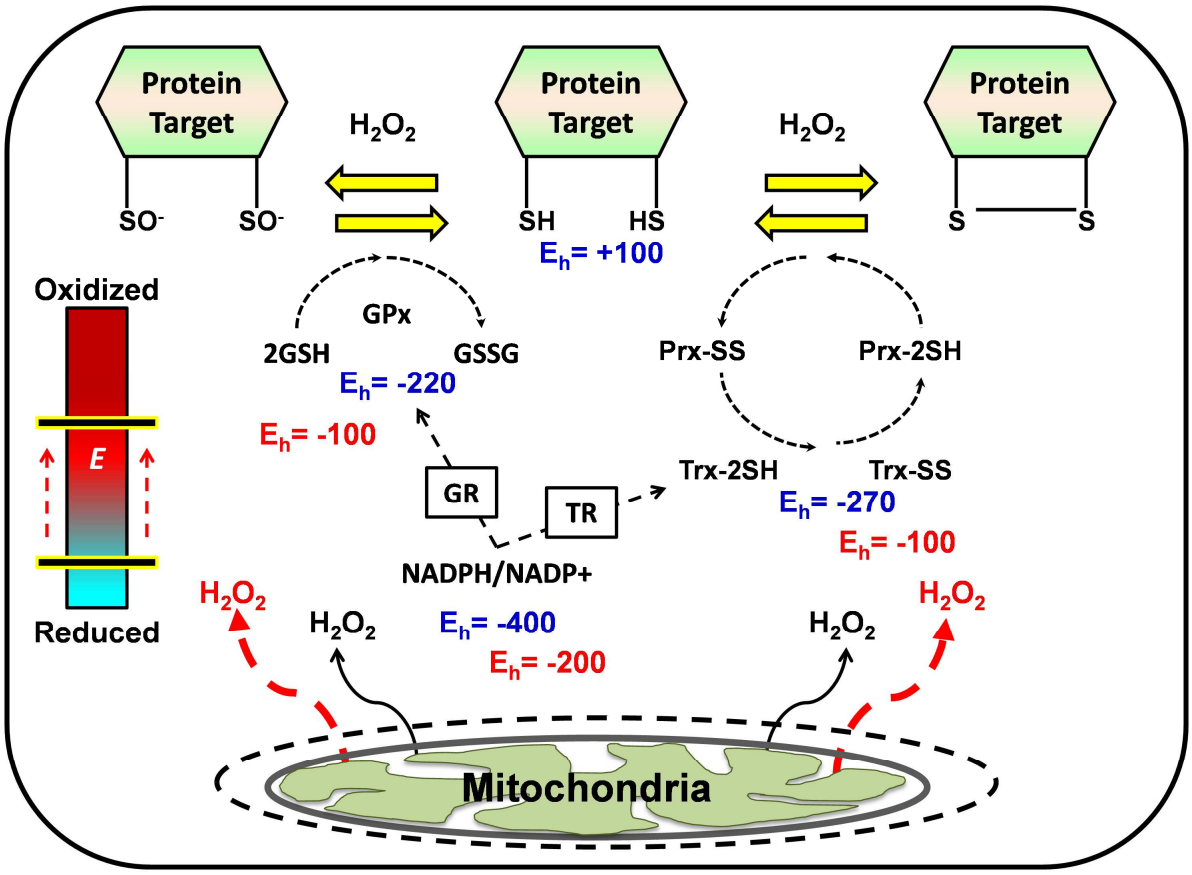

CHAPTER 2: AN OXIDATIVE SHIFT IN MITOCHONDRIAL REDOX REVEALS PYRUVATE DEHYDROGENASE AS A MAJOR H_2O_2 EMITTING SOURCE

Abstract

Once regarded as “byproducts” of aerobic metabolism, the production of superoxide/H_2O_2 is now understood to be a highly specialized and extensively regulated process responsible for exerting control over a vast number of thiol-containing proteins, collectively referred to as the redox-sensitive proteome. Although disruptions within this process, secondary to elevated peroxide exposure, have been linked to disease, delineation of the sources and mechanisms regulating this increased peroxide burden remain poorly defined and as such difficult to target using pharmacotherapy. Here we demonstrate a role for pyruvate dehydrogenase (PDH) as a key source of H_2O_2 under physiological constraints in which respiratory chain-dependent electron leak is negligible. PDH is shown to generate H_2O_2 as a function of glutathione content, antioxidant reductase activity, as well as matrix metabolic balance. These findings suggest a novel and pivotal role for PDH as a redox-sensitive reporter of matrix redox buffering integrity and nutrient status.

Highlights

- Matrix glutathione depletion reveals PDH as a major source of H_2O_2 production
- H_2O_2 production by PDH depends on the redox state of its E2-bound lipoyl groups
- NNT deletion reveals a functional link between PDH and the redox buffering networks
- PDH is a continual source of H_2O_2 even under maximal ADP-stimulating conditions

Introduction

Numerous pathological conditions ranging from cancer to diabetes are associated with elevated reactive oxygen species (59). Specific cause and effect relationships however have proven difficult to establish due to the limited, albeit ever-improving, mechanistic understanding of redox-mediated processes *in vivo*. At present, the intracellular redox environment is envisaged as a network of interconnected redox couples which terminally distribute electrons to the estimated 22,000 redox-sensitive thiols throughout the proteome (13, 33). Disequilibrium between redox couples (i.e., reduction potentials), and thus electron flow, is made possible by continuous input into the reductive (NADPH) and oxidative (O_2, H_2O_2) arms of the system, thus giving rise to the term “redox circuits” (29). Mitochondria play a central role in this system by providing both a major source of the reductive power (e.g., NADPH) as well as the effective counterbalance (e.g., H_2O_2) that dissipates and thus regulates the charge. In fact, it is the regulation of flux through the redox circuitry that is thought to be the mechanism by which H_2O_2 serves as a secondary messenger within biological systems (1, 28). Identification of the primary sources of H_2O_2, as well as the physiological conditions regulating its production rate, is therefore paramount to deciphering the underlying mechanisms responsible for the ever-expanding list of diseases with a redox-mediated etiological component.

In mammalian mitochondria, currently identified sites of electron leak/superoxide formation in the electron transport system (ETS) include the flavin mononucleotide and ubiquinone binding site within complex I, the quinone at centre “o” within complex III, the quinone binding site within glycerol-3-phosphate dehydrogenase, and the electron

transferring flavoprotein Q oxioreductase (6). Superoxide production is membrane potential (ΔΨ)-dependent, meaning that electron leak accelerates dramatically when the reducing pressure within the ETS, and thus ΔΨ, increases (i.e., becomes more negative) due to elevated reducing equivalent supply (i.e., $NADH/NAD^+$, $FADH_2/FAD^+$) relative to demand. Thus, the ETS functions as a gauge of cellular energy balance, accelerating electron leak and H_2O_2 emission when energy supply exceeds demand (2, 22)). H_2O_2 in turn is dismutated to H_2O by reduced glutathione and thioredoxin, both of which are critical to generating and maintaining the reduction of protein thiols (48, 61). Thus in effect, H_2O_2 dissipates the charge distributed throughout the proteome and is therefore thought to be critical to the regulation of various cell processes (29), including insulin sensitivity (13).

In addition to the ETS, several non-respiratory chain sites of superoxide production have been identified including the matrix dehydrogenase enzyme complexes pyruvate dehydrogenase (PDH) and α-ketoglutarate dehydrogenase (αKGDH), both of which are believed to generate H_2O_2 via interactions between the dihydrolipoyl transacetylase (E2) and the FAD-containing dihydrolipoamide dehydrogenase (E3) components of their respective enzyme complexes (53). However, absolute rates of H_2O_2 production by PDH and αKGDH are very low, and thus the extent to which either enzyme contributes to H_2O_2 production in a physiological context has not been clear (6). While investigating the potential influence of redox state on H_2O_2 production at different sites, we were surprised to find that pyruvate-supported H_2O_2 production by PDH is remarkably sensitive to mitochondrial GSH depletion, generating rates of H_2O_2 emission far greater than any other site/substrate combination tested. Subsequent experiments

conducted with isolated enzyme, permeabilized mitochondria, and permeabilized skeletal muscle fiber bundles from multiple species reveal a novel regulatory network between the PDH complex and the mitochondrial redox environment, the implications of which establish PDH as a critical control node within the intracellular redox network reporting on both the nutrient status and redox balance present within the mitochondrial matrix.

Results

Site-specific H_2O_2 emission: Effects of mitochondrial uncoupling and GSH depletion.

To directly compare rates of electron leak from known sites within mitochondria, H_2O_2 emission was monitored in mouse permeabilized skeletal muscle fiber bundles under a variety of substrate combinations. As expected (3, 52), succinate, which feeds electrons directly into the Q-pool and induces reverse electron flow back into complex I, generated H_2O_2 emission rates higher than all other substrate combinations tested. Surprisingly however, pyruvate alone (i.e., no malate) also generated a substantial rate of H_2O_2 emission (Figure 3A). These experiments were carried out under non-ADP-stimulated conditions (i.e., state 4) which favors ETS-supported H_2O_2 emission (e.g., complexes I and III) due to high membrane potential across the mitochondrial inner membrane. As expected, addition of the chemical uncoupler trifluorocarbonylcyanide phenylhydrazone (FCCP), which accelerates proton conductance and lowers membrane potential, eliminated ETS-derived H_2O_2 emission (e.g., glutamate/malate and succinate, Figures 3B & 3C). In contrast, FCCP increased H_2O_2 emission in the

presence of α-ketoglutarate, glycerol-3-phosphate and pyruvate (compare Figure 3C to 3A), suggesting that at least a portion of mitochondrial H_2O_2 production/emission is insensitive to membrane potential and generated by the dehydrogenases themselves.

To determine the potential sensitivity of H_2O_2 emission to an oxidative shift in the mitochondrial redox environment, permeabilized fiber bundles were pre-treated with the glutathione (GSH)-depleting agent 1-chloro-2,4-dinitrobenzene (CDNB). Catalyzed by glutathione S-transferase, CDNB forms an irreversible conjugate with GSH, resulting in a gradual depletion of GSH (19, 58). Compared to GSH-replete fibers, partial depletion (~75%) of GSH did not significantly increase H_2O_2 emission when fibers were energized with glutamate/malate, palmitoyl-L-carnitine, α-ketoglutarate, glycerol-3-phosphate, or succinate (Figure 3F). In stark contrast, when respiration was supported solely by pyruvate, H_2O_2 emission rate increased by more than 20-fold (13.2 ± 1.4 (Fig 3A) vs 281.2 ± 26.8 (Fig 3F) pmol/min/mg dry wt). These rates were higher than all other substrate combinations, including succinate (Figure 3E), and occurred in the absence of any difference in pyruvate-supported O_2 consumption or NADH production (Supplemental Figures 1A & 1B).

Pyruvate-supported *J*H_2O_2 shows striking sensitivity to GSH depletion across species.

To determine if pyruvate-supported H_2O_2 emission is responsive to more physiological declines in GSH, rates of H_2O_2 emission were assessed in fibers pre-treated with varying concentrations of CDNB. As little as ~6% depletion in GSH generated a significant increase in pyruvate-supported H_2O_2 emission, with values rising

exponentially as GSH levels continued to fall (Figure 3G). This striking sensitivity to GSH depletion was also evident in permeabilized skeletal muscle fiber bundles prepared from Sprague-Dawley rats (Figure 3H) and human subjects (Figure 3I). Interestingly, higher concentrations of CDNB were required in rat and human fibers to induce a comparable level of GSH depletion as that seen in mice, perhaps reflecting inter-species differences in total GSH content and/or glutathione-S-transferase expression/activity. These findings reveal PDH as a potential major site of H_2O_2 production that is extremely sensitive to the mitochondrial redox buffering network.

PDH generates H_2O_2 directly via interactions between the E2 and E3 domains.

Mammalian PDH is comprised of three main catalytic components (E1, pyruvate dehydrogenase; E2, dihydrolipoyl transacetylase; E3, FAD-containing dihydrolipoyl dehydrogenase), which combine to form a large (~9.5 MDa) multi-subunit holoenzyme with a stoichiometry of 40:40:20 (E1:E2:E3) (7). To investigate the mechanisms regulating H_2O_2 production in relation to catalytic flux (Figure 4A), experiments were carried out using isolated enzyme. PDH generated substantial rates of H_2O_2 in both the forward (i.e., pyruvate as substrate, Figure 4B) and reverse (i.e., NADH as substrate, Figure 4C) directions. It should be noted that NADH concentrations in excess of 10 μM were found to interfere with the Amplex Ultra Red/HRP detection system (Supplemental Figure 3D). Inclusion of N-ethylmaleimide (NEM), an inhibitor of E2 (9), eliminated pyruvate-supported H_2O_2 production (Figure 4D & 4E). NEM reacts with reduced thiols to form a covalent thioether bond, suggesting that forward electron flux through the sulfhydryls of E2 is required to induce electron leak from the PDH complex.

Subsequent addition of NADH elicited a partial increase in H_2O_2 production, suggesting electron leak from the E3 component. In separate experiments, inclusion of the irreversible flavoprotein inhibitor diphenyliodonium chloride to block E3 generated a partial increase in H_2O_2 production with pyruvate as substrate. Inhibition of both E2 and E3 completely eliminated H_2O_2 production with either pyruvate or NADH as substrate. These findings suggest that both the E2 and E3 components contribute to H_2O_2 production by the PDH complex.

Exogenous superoxide dismutase (SOD) was included in the preceding experiments to ensure superoxide produced by the PDH complex was converted to H_2O_2. Surprisingly, omission of SOD did not affect pyruvate-supported H_2O_2 production (Figure 4F) whereas inclusion of catalase eliminated the signal (Figure 4G), suggesting the PDH complex is producing H_2O_2 directly. This is not without precedent as certain isoforms of NADPH oxidase (36) and xanthine oxidase (32) have also been shown to generate H_2O_2 directly.

Isolated PDH generates H_2O_2 primarily as a function E2 “reducing pressure”.

Reducing pressure within the E2 component of PDH is determined by the redox state of its bound lipoyl groups. These lipoyl moieties oscillate between reduced dihydrolipoate (DHLA) and oxidized lipoate (LA) during the course of enzymatic turnover. Reduction to DHLA is determined by the rate of pyruvate decarboxylation at E1 in combination with the acetyl transferase activity of E2. Reoxidation of DHLA following acetyl-CoA release is mediated by the FAD-containing dehydrogenase component (E3) of the PDH complex via an NAD^+-dependent mechanism (Figure 4A).

It was therefore hypothesized that PDH-supported H_2O_2 may be dependent on the ratio of DHLA/LA, thus generating a maximal rate of H_2O_2 when pyruvate and CoA are saturating in the absence of NAD^+. To test this hypothesis, PDH-supported JH_2O_2 was measured in response to increasing concentrations of pyruvate either in the absence (Figure 5A) or presence (Figure 5B) of NAD^+. As anticipated, NAD^+ decreased the H_2O_2 V_{max} by ~50% and increased the pseudo K_m ([pyruvate] generating half H_2O_2 V_{max}) by greater than 60-fold compared to the no NAD^+ condition. These data imply that an inability of E3 to regenerate LA following reduction dramatically increases the sensitivity of the complex to pyruvate with respect to generation of H_2O_2. To further assess the influence of NAD^+, PDH-mediated H_2O_2 production was continuously monitored while titrating NAD^+ and holding the pyruvate concentration constant (1 mM). NAD^+ decreased pyruvate-supported JH_2O_2 in a dose-dependent fashion with an IC_{50} of approximately ~3 μM (Figure 5C), confirming the dependence of PDH on NAD^+ as an electron acceptor and providing further evidence of the direct influence of reducing pressure on PDH-mediated H_2O_2 production.

Under physiological conditions, the ratio of NADH/NAD^+ varies as a function of metabolic balance. To assess the influence of dynamic fluctuations in NADH/NAD^+ on PDH-mediated H_2O_2 generation, pyruvate-supported JNADH and JH_2O_2 were monitored in parallel under identical substrate conditions. The starting NAD^+ concentration for these assays was 50 μM (~K_m for JNADH; data not shown). Upon addition of pyruvate (1 mM), NAD^+ was rapidly converted to NADH (Figure 5D blue trace), gradually leveling off after ~10 min at a maximum concentration of ~28 μM and a ratio of NADH/NAD^+ slightly >1. By contrast, the rate of H_2O_2 production by PDH

appeared to increase in direct proportion to the rise in NADH (Figure 5D, red trace). When calculated [H_2O_2]and [NADH] were converted to point by point production rates, the flux derivations were near mirror images of one another (Figure 5E). The addition of oxaloacetate (5 mM) following this initial 10 minute period led to non-enzymatic conversion of oxaloacetate to malate at the expense of NADH, effectively regenerating NAD^+ and drastically decreasing JH_2O_2. Interestingly, the rate of H_2O_2 production in the presence of oxaloacetate was similar to that observed during the first 30 seconds following pyruvate addition prior to any substantial elevations in NADH (Figure 5F); again consistent with the notion that NAD^+-mediated re-oxidation of DHLA is a critical determinant of PDH-mediated H_2O_2 production.

Although the availability of NAD^+ is critical to the re-oxidation of the E2 component, a majority of flux control through the PDH complex is thought to be exerted by phosphorylation of the E1 component which inactivates the enzyme (26). Incubation of isolated PDH with recombinant pyruvate dehydrogenase kinase 4 (PDK4), the most active PDK isoenzyme in skeletal muscle, as expected elicited a decrease in NADH production (Figure 5G), indicative of reduced flux through the complex. PDK4 also induced a parallel decrease in H_2O_2 production, supporting the concept that the E1-catalyzed reduction of E2 bound lipoate is necessary for H_2O_2 generation. To further examine the influence of flux control through PDH on H_2O_2 production, permeabilized skeletal muscle fiber bundles were prepared from wildtype and $PDK4^{-/-}$ mice (27). As expected, pyruvate-supported JO_2 consumption was elevated under state 4 conditions in fibers from $PDK4^{-/-}$ compared with wildtype mice (Figure 5H) and was matched by a nearly identical increase in JH_2O_2 production (Figure 5I). Taken together, these data

suggest that the rate of H_2O_2 generation by the PDH complex reflects the reducing pressure within the E2 component of the complex which is determined, at least in part, by the E1 catalytic flux rate relative to the ratio of $NADH/NAD^+$.

Carnitine elevates pyruvate-supported O_2 flux/NADH production and lowers H_2O_2 emission by up-regulation of redox buffering.

Flux through the PDH complex is also subject to direct allosteric inhibition by accumulation of acetyl-CoA, the product of the E2 reaction. Acetyl-CoA accumulates in the mitochondrial matrix when entry into the TCA cycle is limited by the availability of anaplerotic substrates (e.g., oxaloacetate) for the citrate synthase reaction. In striated muscle, the accumulation of acetyl-CoA is counterbalanced by the activity of carnitine acetyltransferase (CrAT), a mitochondrial enzyme that converts excess acetyl-CoA to membrane permeable acetylcarnitine esters which may then efflux out of the organelle and cell (40). To investigate how flux through PDH may be integrated with flux through other metabolic pathways to regulate JH_2O_2 production by PDH, a series of experiments were performed using permeabilized skeletal muscle fiber bundles. In agreement with previous findings (40), addition of carnitine to permeabilized fibers energized with pyruvate alone markedly increased JO_2 consumption (Figure 6A) and JNADH production (Figure 6B), consistent with a CrAT-catalyzed relief of acetyl-CoA-mediated inhibition of PDH. Based on the increase in JH_2O_2 observed when flux through PDH was increased by the ablation of PDK4 (Figure 5I), it was anticipated JH_2O_2 would also increase in response to a carnitine-mediated increase in flux through PDH. Surprisingly however, addition of carnitine decreased pyruvate-supported mitochondrial JH_2O_2

emission, a response that was particularly evident in fibers pretreated with increasing concentrations of CDNB to reduce matrix GSH (Figure 6C). In other words, the extremely high PDH-mediated JH_2O_2 evident in GSH-depleted fibers (e.g., Figure 3) was markedly attenuated when flux through PDH was increased by addition of carnitine. This suggested that the net rate of H_2O_2 generation by PDH does not simply reflect a balance between flux through the complex and buffering of the H_2O_2 by GSH, but may involve a more complex relationship with the matrix redox buffering system. To test this possibility, experiments were repeated in the presence of inhibitors of both glutathione reductase (bis-chloroethylnitrosourea, BCNU) and thioredoxin reductase (auranofin, AF) without depleting matrix GSH. Under these conditions, the ability of carnitine to suppress PDH-mediated JH_2O_2 emission (i.e., pyruvate sole substrate) was eliminated; in fact, addition of carnitine generated a marked increase, not a decrease, in pyruvate-supported JH_2O_2 emission (Figure 6D & 6E). Of note, even prior to the addition of carnitine, pyruvate-supported JH_2O_2 emission was ~2-fold higher in BCNU/AF treated versus non-treated fibers, reflecting the absence of input from the redox buffering network. This apparent dependence on the matrix redox buffering system was confirmed in a similar series of experiments performed on permeabilized fibers from wildtype and muscle-specific CrAT null mice ($CrAT^{M-/-}$). Addition of carnitine increased flux through PDH (i.e., increased state 4 JO_2, Supplemental Figure 2A) and decreased H_2O_2 emission in permeabilized fibers from wildtype mice with an intact redox buffering system (Figure 6F open bars, similar to 6C). However, when both arms of the matrix redox buffering system were blocked (+BCNU/AF), addition of carnitine increased JH_2O_2 emission by PDH (Figure 6G open bars, similar to 6E). In the absence of CrAT

(i.e., permeabilized fibers from CrAT$^{M-/-}$), the ability of carnitine to reduce PDH-mediated JH_2O_2 emission with an intact buffering system (Figure 6F), and by contrast to increase JH_2O_2 emission when redox buffering was inhibited (Figure 6G), were both lost, confirming the effects of carnitine were mediated by CrAT activity. Finally, when malate was used in place of carnitine to facilitate entry of acetyl-CoA into the TCA cycle and thereby accelerate PDH flux (i.e., increase in state 4 JO_2, Supplemental Figure 2B), PDH-mediated JH_2O_2 emission decreased when the redox buffering system was intact, but increased dramatically when the redox buffering system was blocked (Figure 6H-I).

Collectively, these findings suggest that flux through the PDH complex is coupled to the matrix redox buffering system, the integration of which appears to be playing a major role in determining the net rate of H_2O_2 generation by PDH. It is important to note that the difference in pyruvate-supported JO_2 observed in permeabilized fibers from PDK4$^{-/-}$ versus wildtype mice (Figure 5H) was only a fraction of the increase in JO_2 observed in permeabilized fibers from wildtype mice in the presence of carnitine or malate (Supplemental Figures 2A and 2B). This indicates that with pyruvate as the sole substrate, the rate of NADH production was insufficient to support state 4 respiration in permeabilized fibers from PDK4$^{-/-}$ mice, most likely due to allosteric inhibition of PDH by acetyl-CoA. However, when acetyl-CoA accumulation was prevented by addition of carnitine (acetyl-CoA conversion to acetylcarnitine via CrAT) or malate (acetyl-CoA entry into the TCA cycle), the rate of NADH production by PDH was fully sufficient to support state 4 respiration. This led us to speculate that JNADH generation may be a key factor coupling PDH to the matrix redox buffering systems and thus the control of H_2O_2 generation by the PDH complex.

Functional nicotinamide nucleotide transhydrogenase is required for carnitine-induced depressions in PDH-supported JH_2O_2.

The mitochondrial glutathione and thioredoxin redox buffering systems derive their reducing potential from NADPH. The principle source of NADPH in the matrix is nicotinamide nucleotide transhydrogenase (NNT), an inner mitochondrial trans-membrane protein that utilizes the proton gradient across the inner mitochondrial membrane to drive the otherwise thermodynamically unfavorable regeneration of NADPH from NADH (25, 43). Thus, NADH is both a substrate for NNT and a source of fuel for the ETS to generate the membrane potential needed by NNT. It was therefore reasoned that the rate of NADH generation may be critical to the rate at which NADPH regeneration can be maintained by NNT, and therefore the rate at which the glutathione and thioredoxin reductase reactions can be supported to regenerate GSH and buffer H_2O_2 produced by PDH. To test this hypothesis, membrane potential was lowered by addition of FCCP to permeabilized fiber bundles respiring on pyruvate alone. In contrast to the decrease in pyruvate-supported H_2O_2 emission observed upon addition of carnitine under state 4 respiratory conditions (i.e., when membrane potential is high; Figure 6C and 6F), addition of carnitine during uncoupled respiration (+FCCP) induced higher rates of H_2O_2 emission (Figure 7A), providing at least indirect evidence that loss of membrane potential limits NNT activity and buffering of PDH-mediated JH_2O_2. To directly determine the dependence of PDH-mediated JH_2O_2 on NNT activity, pyruvate-only-supported JH_2O_2 emission was measured in permeabilized fiber bundles from C57BL/6J mice, which lack functional NNT (16, 57), and compared with permeabilized

fibers from C57BL/6N mice, which express functional NNT. Pyruvate only supported JH_2O_2 emission was higher in permeabilized fibers from C57BL/6J mice and addition of carnitine sharply increased JH_2O_2 emission (Figure 7B & 7C), similar to the response observed when matrix redox buffering was compromised by inhibition of both glutathione and thioredoxin reductase (Figure 6E). These findings indicate that H_2O_2 production by PDH is a function of the coupling between PDH-mediated *J*NADH and NNT-mediated *J*NADPH. While NNT accounts for ~50% of matrix NADPH formation (46), other potential sources include the $NADP^+$-dependent isocitrate dehydrogenase 2 and $NADP^+$-dependent malate dehydrogenase (i.e., malic enzyme). Indeed, addition of malate completely abrogated the carnitine-induced increase in JH_2O_2 in permeabilized fibers from C57BL/6J mice (Figure 7D), suggesting that provision of a source of NADPH alternative to NNT was able to restore the coupling between the matrix redox buffering systems and regulation of PDH-mediated H_2O_2 production. That the effect of malate was mediated by NADPH was confirmed by addition of BCNU and AF to block matrix redox buffering, which completely eliminated the rescue effect of malate (Figure 7D, +BCNU/AF).

Manipulation of matrix redox buffering reveals PDH as the principle source of H_2O_2 during maximal state 3 respiration.

The C57BL/6J mice in combination with carnitine provide a unique model whereby H_2O_2 emission derived specifically from the PDH complex can be assessed in the absence of redox buffering, as well as at varying levels of reactivity. Using this approach it was possible to design experiments to determine the impact of $NADH/NAD^+$

on pyruvate-supported H_2O_2 emission under physiological constraints (i.e., ADP-stimulated conditions in the absence of respiratory inhibitors). As anticipated based on the isolated enzyme experiments (Figure 5E), the addition of ADP to permeabilized fibers prepared from C57BL/6J mice energized with pyruvate and carnitine led to a dose-dependent decrease in H_2O_2 emission (Figure 8A), presumably reflecting the consequence of a progressive decrease (i.e., oxidation) in NADH/NAD^+ ratio (Figure 5C & 5E). It is important to point out that even under maximal ADP stimulated conditions when H_2O_2 production by the ETS is negligible (i.e., <1 pmol/min/mg dry wt, analogous to +FCCP for GM and S in Fig 3B and 3C), PDH is still capable of producing substantial rates of H_2O_2 (~22 pmol/min/mg dry wt).

Lastly, to estimate the potential contribution of H_2O_2 production by PDH relative to the ETS in a physiological context, a series of JO_2 production and JH_2O_2 emission assays were carried out in permeabilized fibers from C57BL/6N mice under non-ADP (state 4) and steady-state ADP-stimulated conditions using a respiratory clamp system. To focus only on H_2O_2 production (i.e., no matrix redox buffering), all JO_2 and JH_2O_2 experiments were carried out in the presence of BCNU and AF. Under state 4 conditions, H_2O_2 produced/O_2 consumed was highest for permeabilized fibers supported by succinate alone, but that rate dropped to near zero upon transition to maximal state 3 conditions (Figure 8B). By contrast, the rate of H_2O_2 produced/O_2 consumed was elevated even under state 3 conditions when permeabilized fibers were supported by pyruvate/carnitine and, to a lesser extent, glutmate/malate (the latter likely reflecting production from glutamate dehydrogenase and/or αKGDH). Taken together, these findings suggest that matrix dehydrogenases are likely a constant source of H_2O_2

production in mitochondria, the potential being greatest for PDH due to its sensitivity to the redox buffering system.

Discussion

Establishment and maintenance of cellular redox circuitry is dependent upon continual generation (NADPH) and dissipation (H_2O_2) of reducing potential within the mitochondrial and cytosolic compartments. The results contained herein reveal the PDH complex as a pivotal sensor and regulator within the redox circuitry system that integrates with the matrix redox buffering system and metabolic state of the cell to regulate H_2O_2 production. In this context, there are three main findings from the present study. First, PDH was shown to generate H_2O_2 directly at a rate responsive to the metabolic balance of the cell (i.e., NADH/NAD^+), to the downstream flux rate of the reaction product (i.e., acetyl-CoA), and, perhaps most striking, to the integrity of the redox buffering system. The dramatic sensitivity of PDH to declines in matrix GSH content was particularly interesting in that the effect was unique to PDH. Moreover, pyruvate-supported H_2O_2 emission gradually increased to rates exceeding all other substrate combinations. Second, the rate of H_2O_2 emission from PDH was found to be under the direct influence of the redox buffering network through an NNT-mediated self-quenching mechanism. These findings reveal the dynamic interactions between NADH-linked dehydrogenases and the matrix redox buffering network, firmly establishing the importance of NNT in the maintenance of matrix reducing power (i.e., NADPH supply) and control of peroxide emission. Lastly, manipulation of the redox buffering network unveiled PDH, and to a lesser extent other matrix soluble dehydrogenases, as

significant and constant sources of H_2O_2 production even under ADP-stimulating conditions. To our knowledge, this is the first evidence of mitochondrial H_2O_2 production under state 3 conditions, suggesting that the matrix dehydrogenases contribute substantially to the overall peroxide burden. Collectively, these findings reveal an extremely sensitive and exquisitely balanced network between the PDH complex and the redox buffering system that both senses and responds to reducing pressure in accordance with the overall state of the mitochondrial redox environment. This supports a novel paradigm, exemplified by the PDH complex, in which control of the redox environment is exerted and dominated by the redox buffering network rather than simply production of reactive oxygen species.

In the present investigation, PDH was found to generate H_2O_2 as a function of NADH/NAD^+ in a manner that was independent of mitochondrial membrane potential. The dependence/independence of H_2O_2 production on membrane potential is difficult to determine in an intact system, due in part to the lack of a specific inhibitor of NADH oxidation at complex I. Use of any ETS inhibitor downstream of complex I (e.g., rotenone, antimycin A, cyanide) will also lead to an increase in mitochondrial NADH/NAD^+, which clearly impacts PDH-mediated H_2O_2 generation (Figure 5). Thus, experiments designed to identify the source of H_2O_2 in permeabilized fibers had to be performed in the absence of inhibitors and interpreted in the context of the ETS. Indirect evidence for PDH as the primary source of H_2O_2 during pyruvate-stimulated conditions was provided by comparing the impact of FCCP and ADP between pyruvate and succinate energized conditions. Succinate-supported H_2O_2 is generated from site IQ of complex I due to reverse electron flow from complex II (i.e., succinate

dehydrogenase) (6), as well as a small contribution from the flavin moiety of succinate dehydrogenase itself (45), both of which are highly dependent on membrane potential. Indeed, confirming previous findings (3), succinate-supported H_2O_2 emission in permeabilized fibers was high under state 4 conditions, but completely eliminated when membrane potential was reduced by transition to state 3 (Figure 8B) or addition of the uncoupler FCCP (Figure 3C). By contrast, pyruvate-stimulated JH_2O_2 emission remained significantly elevated under both maximal ADP- and FCCP-stimulated conditions, indicative of independence from mitochondrial membrane potential. It is of interest to note that the absolute rate of pyruvate-supported JH_2O_2 emission was nearly identical under both respiratory conditions (~22 pmol/min/mg dry wt), despite the fact the experiments were conducted in permeabilized fibers from two different strains of mice with vastly different rates of pyruvate-stimulated H_2O_2 production rates under state 4 conditions. In permeabilized fibers with an intact redox buffering system (i.e, from C57BL/6N), pyruvate-supported JH_2O_2 emission increased from ~15 pmol/min/mg dry wt in state 4 to ~22 pmol/min/mg dry wt in response to FCCP (Figure 3A and 3C), most likely reflecting the balance between the increase in flux through the PDH complex and redox buffering capacity independent of membrane potential (i.e., +FCCP). In permeabilized fibers inherently lacking membrane potential-dependent redox buffering (i.e., from C57BL/6J), pyruvate supported H_2O_2 emission was ~65 pmol/min/mg dry wt in state 4, then decreased to ~22 pmol/min/mg dry wt under maximal state 3 conditions (Figure 8A). In this case, ADP titration gradually decreased pyruvate-supported JH_2O_2, most likely as a function of the oxidation of NADH/NAD^+, eventually achieving the same

balance in flux through the PDH complex and net JH_2O_2 emission as in C57BL/6N fibers +FCCP.

The remarkably divergent effects of carnitine on pyruvate-supported H_2O_2 production in fibers from C57BL/6N vs C57BL/6J mice reveal a dynamic interplay between the PDH complex and the redox buffering system. Addition of carnitine to fibers with a functional NNT system increased pyruvate-supported JO_2 and lowered H_2O_2 emission, consistent with relief of acetyl-CoA-mediated inhibition of PDH due to accelerated conversion of surplus acetyl-CoA to acetyl-carnitine and efflux out of the mitochondria (40). However, addition of carnitine to fibers lacking functional NNT generated a similar increase in JO_2 but a marked increase in pyruvate-supported H_2O_2 emission. These findings suggest that flux through the PDH complex normally generates sufficient reducing power (i.e., NADH) to support NNT activity, keeping H_2O_2 emission by PDH in check. In the absence of NNT however, reliance is limited to non-membrane potential dependent sources of NADPH (i.e., IDH and matrix malic enzyme), creating a limitation in the redox buffering system and thereby shifting the relationship between catalytic flux and net H_2O_2 emission by the PDH complex. This emphasizes the importance of the redox buffering system to determining the overall impact of a given redox burden. From an experimental design perspective, it is obvious divergent conclusions would have been drawn had either the C57BL/6N or C57BL/6J strains been used exclusively. These findings also raise the distinct possibility that the reduced redox buffering capacity of the C57BL/6J strain contributes to its increased susceptibility to diet-induced insulin resistance, emphasizing the point that genetic models developed on the C57BL/6J background must be interpreted in the context of the NNT deletion.

The dependence of PDH-derived H_2O_2 on matrix GSH content is a novel finding, as no other site was found to respond in a similar fashion, including αKGDH which is nearly identical structurally to PDH. The level of decrease in GSH necessary to trigger an increase in H_2O_2 emission (~6-25% depletion) is observed in a variety of pathological conditions thought to have a reactive oxygen species-mediated component in their etiology, including diet-induced insulin resistance, diabetes, and aging (2, 50, 51). The dependence of PDH-derived H_2O_2 on GSH appears to be specific to the glutathione molecule itself rather than direct interaction with a redox buffering enzyme-coupled system, as inhibition of both glutathione and thioredoxin reductases in the absence of GSH depletion only modestly increased pyruvate-supported H_2O_2 emission. These findings imply the existence of some form of direct GSH-mediated scavenging and/or physical association with the PDH complex. With respect to the latter, the E2-bound lipoyl moieties within the PDH complex are prime targets for glutathionylation, and indirect evidence for both reversible glutathionylation of the lipoyl groups bound to E2 in αKGDH (4), as well as direct interaction with thioredoxin and glutathione (8), have been reported. However, using a direct immunoblotting approach (10, 31), we were unable to detect glutathionylation of the E2 component of PDH under several different experimental conditions (data not shown), supporting the former notion that GSH is functioning as a direct scavenger of H_2O_2 within the complex. In this context, it is intriguing to consider the possibility that the high abundance of E2-bound lipoyl groups (3/E2 x 40 E2 = 120/PDH complex) may provide a source of reducing power to directly regenerate GSH from GSSG, creating an internal redox buffering circuit to counterbalance H_2O_2 production by the complex. Such a mechanism could also protect

against irreversible inactivation of E1 by lipoate thiyl radicals that form when the complex is under elevated reducing pressure, a self-regulatory mechanism that has been observed in the αKGDH complex (8, 9).

In aggregate, a potentially pivotal role of the PDH complex in mitochondrial and cellular redox circuitry has been indentified, highlighting the mechanisms distinguishing H_2O_2 production from H_2O_2 emission by the complex. H_2O_2 production is determined by the reducing pressure exerted on the E2 lipoate residues, which in turn is dictated by the forward catalytic flux rate through the decarboxylation (E1) and transacetylation (E2) reactions relative to the NADH/NAD^+ ratio. Supply of pyruvate, as well as established allosteric (i.e., ↑ [acetyl-CoA]) and covalent (i.e., PDK-catalyzed phosphorylation) feedback mechanisms, regulate forward catalytic flux and thus the reducing 'pressure head', while availability of NAD^+ determines the degree to which the pressure head is relieved. Evidence suggests that GSH directly buffers H_2O_2 produced and is therefore crucial to determining the net rate of H_2O_2 emission by the PDH complex. Under most circumstances, regeneration of GSH keeps pace with H_2O_2 production due to the glutathione and thioredoxin redox systems, both of which derive their reducing power from NNT-mediated NADPH in the presence of a functional ETS and source of NADH. The NADH needed for the NNT reaction, as well as the ETS, is at least in part supplied by the PDH reaction, thus creating a closed loop system allowing the PDH complex to buffer its own H_2O_2. Interestingly, loss of this redox buffering system in and of itself does not appreciably increase pyruvate-supported H_2O_2 emission, but rather is likely to decrease the ability of the redox buffering cycle to maintain a GSH:GSSG ratio sufficient to fully buffer H_2O_2 and thus maintain protein cysteine redox status under a given rate of

reductive pressure. To place in a physiological context, the implication is that conditions in which matrix GSH:GSSG ratio and/or total GSH content are reduced due to nutrient overload (e.g., high fat diet) (2), and/or the mitochondrial redox buffering system is compromised due to aging or disease (50, 51), will generate a net increase H_2O_2 emission for a given degree of reductive pressure on the E2-bound lipoyl of the PDH complex.

Experimental Procedures

Animals and Reagents

All animal studies were approved by the East Carolina University Institutional Animal Care and Use Committee. Male Sprague-Dawley rats (12-16 weeks old) and C57BL/6N mice were purchased from Charles River Laboratory. C57BL/6J were purchased from Jackson Laboratory. $CrAT^{M-/-}$ were initially generated on a C57BL/6J background (40) and backcrossed to a C57BL/6N background for >8 generations (confirmed by genetic background testing, Charles River Laboratory). $PDK4^{-/-}$ mice were generated on a C57BL/6J background as described (27). All rodents were housed in a temperature (22˚C) and light controlled (12 hour light/12 hour dark) room and maintained on standard chow with free access to food and water. For all experiments, rodents were fasted 4 hours, anesthetized, and red portions of the gastrocnemius muscle dissected and separated into fiber bundles. Remaining portions of muscle were frozen (liquid N_2) for later analysis. All reagents and chemicals were obtained from Sigma-Aldrich (including PDH from porcine heart and anti-protease cocktail) with the exception of

Amplex Ultra Red reagent (Invitrogen), GSH/GSSG assay kit (Oxis International Inc.), and recombinant PDK4 (Mitosciences).

Preparation of permeabilized fiber bundles

This technique is partially adapted from previous methods and has been thoroughly described (44). For experiments involving GSH depletion, 1-Chloro-2,4-dinitrobenzene (CDNB) or ethanol was added during saponin permeabilization. Following permeabilization, fibers were washed in ice-cold buffer Z (K-MES [110 mM], KCl [35 mM], EGTA [1 mM], K_2HPO_4 [5 mM], $MgCl_2$-6H2O [3 mM], BSA [0.5 mg/ml] pH 7.1, 295 mOsm) to remove endogenous substrates and un-reacted CDNB. This method has previously been shown using isolated mitochondria to prevent direct CDNB-derived superoxide generation (58). In addition, CDNB alone was shown to severely interfere with the Amplex Ultra Red/HRP detection system (data not shown), thus further emphasizing the need to wash out all unreacted CDNB prior to experimentation. Confirmation of CDNB washout was inferred based on a lack of increase in resorufin fluorescence during glutamate/malate energized conditions compared to that elicited in fibers which were not exposed to CDNB.

Mitochondrial respiration and H_2O_2 emission measurements

High-resolution O_2 consumption measurements were conducted at 37˚C in buffer Z, supplemented with creatine monohydrate (25mM), using the OROBOROS O_2K Oxygraph. Mitochondrial H_2O_2 emission was measured fluorometrically at 37˚C via Amplex Ultra Red (10 μM) / horseradish peroxidase (HRP: 3 U/ml) detection system

(Ex:Em 565:600). Fluorescence was monitored using a SPEX Fluoromax 3 (HORIBA Jobin Yvon) spectrofluorometer with temperature control and magnetic stirring. For each experiment, resorufin fluorescence was converted to nM H_2O_2 via an H_2O_2 standard curve (Supplemental Figure 3A-B) generated under identical substrate conditions (with the exception of a permeabilized fiber) as employed for each protocol. To this end, all substrates utilized were tested for any potential interference with the Amplex Ultra Red/HRP detection system (Supplemental Figure 3C). Blebbistatin (25 μM) was present during all O_2 consumption and H_2O_2 emission experiments to prevent contraction (44). At the conclusion of each experiment, fiber bundles were washed in double-distilled H_2O to remove salts and freeze-dried in a lyophilizer (Lab-conco). The rate of respiration was expressed as pmol/s/mg dry weight and H_2O_2 emission as pmol/min/mg dry weight.

Mitochondrial NADH production

All NADH production assays were carried in a potassium phosphate based buffer (50 mM), containing $CaCl_2$ (10 μM) and $MgCl_2$ (200 μM), pH 7.4. Permeabilized fibers were prepared as indicated above. Following a 15 minute wash in buffer Z, fibers were incubated with the pore-forming peptide alamethicin (30 μg/ml) in order to permeabilize the inner mitochondrial membrane (53). Experiments were carried out in the presence of coenzyme A (100 μM), NAD^+ (1 mM), thiamine pyrophosphate (300 μM), rotenone (2 μM) and the indicated substrates. NADH production was tracked via auto-fluorescence (Ex:Em 376/450). Fluorescence values were converted to μM NADH via an NADH standard curve.

Isolated PDH experiments

All experiments were carried using PDH from porcine heart (Sigma-Aldrich) in potassium phosphate buffer as described above with the addition of coenzyme A (100 μM) and thiamine pyrophosphate (300 μM). The enzyme concentration for all assays was 16.8 mU/ml. For H_2O_2 emission experiments, buffer was supplemented with Amplex Ultra Red (10 μM) and HRP (3 U/ml). Coenzyme A was found to increase fluorescence, thus all H_2O_2 emission experiments were performed after an 8 minute recording of fluorescence in the absence of substrate. Coenzyme A-induced fluorescence was subtracted out prior to data analysis. NADH production was assessed as stated above. Data are expressed as pmol/s/U.

GSH measurements

Fiber bundles were homogenized in HEPES (3 mM), sucrose (25 mM), and EGTA (0. 5mM), pH 7.2. Buffer was supplemented on the day of experimentation with 1% Triton and an anti-protease cocktail. Total GSH was measured using the reagents and calibration set provided by the GSH/GSSG assay.

Human subjects and tissue biopsy

Three healthy men and 2 women were recruited to participate in this investigation (age 26.2 ± 6.1, BMI 25.2 ± 3.7). None of the subjects had any disease or were taking medications known to alter metabolism. Subjects were given both oral and written information about the experimental procedures before giving their informed consent.

The experiments were approved by the Institutional Review Board of East Carolina University and conducted in accordance with the Declaration of Helsinki principles. On the day of the experiment, subjects reported to the laboratory following an overnight fast (12 hours). Skeletal muscle biopsies were obtained from the lateral aspect of the vastus lateralis by the percutaneous needle biopsy technique under local subcutaneous anesthesia (1% lidocaine) and used to prepare permeabilized fiber bundles.

Statistics

Data are presented as mean ± SEM. Statistical analysis were performed using t-tests or 1-way ANOVA with Student-Newman-Keuls methods for analysis of significance among groups. The level of significance was set at $P < 0.05$.

ACKNOWLEDGEMENTS

This work was supported by funding from the NIH; 1F32AR061946 (LAAG), 1R01DK089312 (D.M.M.), 1R01DK074825 and 1R01096907 (P.D.N.).

Figure 3. Effects of FCCP and GSH depletion on site-specific mitochondrial H_2O_2 emission. Permeabilized fibers were prepared from RG of C57BL/6N mice (**A-C, E-G**), SD rats (**H**), or vastus lateralis from human biopsies (**I**) and pre-treated with varying concentrations of CDNB. H_2O_2 emission rate (JH_2O_2) was assessed in response to glutamate-malate (GM 10 mM-2 mM), palmitoyl-carnitine (PC 25 μM), α-ketoglutarate

(AKG 10 mM), glycerol-3-phosphate (G3P 10 mM), succinate (Succ 10 mM), pyruvate (Pyr 1 mM). Maximal concentrations of FCCP-5 µM were added at the end of each protocol (**A**) *Different from GM, PC, AKG, G3P ($p < 0.05$). **Different from all other substrate combinations ($p < 0.05$). (**B**) Representative H_2O_2 emission experiment in response to Succ and FCCP (left Y-axis) or Pyr and FCCP (right Y-axis). (**C**) Quantified rates (FCCP effect only) from experiment depicted in panel **B**, as well as the remaining substrate combinations. *Different from all other substrate combinations ($p < 0.05$). (**D**) GSH was assessed in fibers pre-treated with varying concentrations of CDNB. Percent values inside bars represent mean percent reductions from the 0 µM condition. *Different from 0 µM condition ($p < 0.05$). (**E**) Representative H_2O_2 emission experiment in response to Succ or Pyr in fibers pre-treated with 1 µM CDNB (dry weights of fibers for each experiment were within 0.01 mg). (**F**) Quantified rates (CDNB effect) from experiment depicted in panel E, as well as the remaining substrate combinations. Numbers above bars represent P values from paired t-tests comparing control (i.e., panel A) to CDNB-treated fibers within a substrate group. *Higher than all other substrate combinations ($p < 0.05$). (**G-I**) Fibers were pre-treated with varying concentrations of CDNB and pyruvate (1 mM) supported H_2O_2 emission was then assessed. GSH data are presented as % change from ethanol control. GSH data from panel **G** was reproduced from **panel D** and expressed as % Change from control. *Different from 0 µM condition ($p < 0.05$). Data are mean ± SEM, n=6/group.

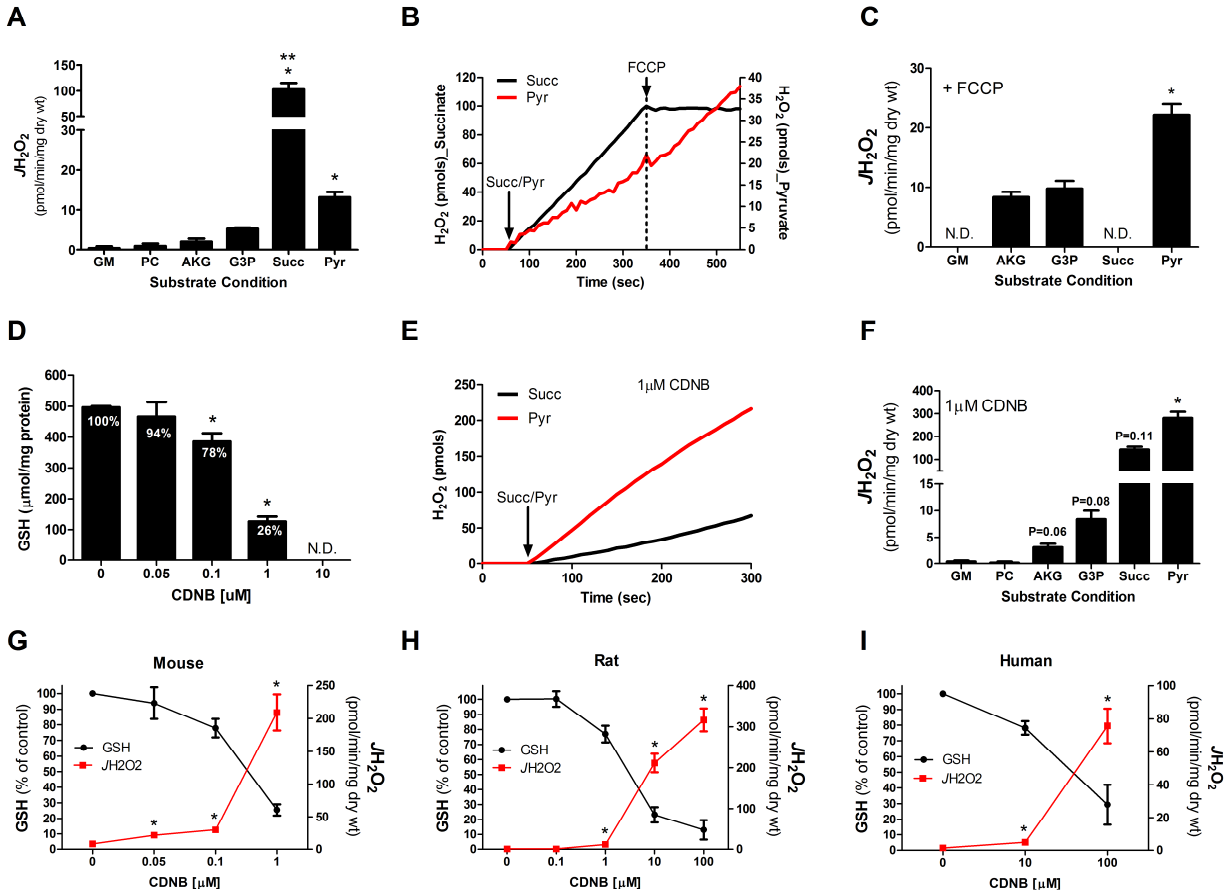
A
B
C
D
E
F
G
H
I
Substrate Condition
GM
PC
AKG
G3P
Succ
Pyr
Succ
Pyr
FCCP
Succ/Pyr
Time (sec)
+ FCCP
N.D.
CDNB [uM]
1μM CDNB
P=0.06
P=0.08
P=0.11
Mouse
Rat
Human
GSH
JH2O2
CDNB [μM]

Figure 4. H_2O_2 production from isolated PDH. (**A**) Cartoon schematic of the PDH reaction: 1. Pyruvate is decarboxlated by E1 to form hydroxyethyl thiamine pyrophosphate (HE-TPP). 2. Hydroxyethyl group is transferred to lipoate and oxidized to form acetyl dihydrolipoate. 3. Acetyl group is transferred to CoA to form acetyl-CoA. 4a. Dihydrolipoate is oxidized back to lipoate via the FAD moiety within E3, 4b. Reduced FAD is oxidized by NAD^+ resulting in the formation of NADH. (**B-G**) Data were generated using PDH from porcine heart. (**B**) Representative H_2O_2 production experiment. Black arrows indicate the addition of pyruvate (1 mM). (**C**) H_2O_2 production in response to increasing concentrations of NADH. (**D**) Representative H_2O_2 production experiment in response to both 1 mM pyruvate and 100 µM NADH following incubation of isolated PDH with 2 mM NEM, 1 mM DPI, or both. (**E**) Quantified rates of production from experiment depicted in panel **D**. (**F**) H_2O_2 production was assessed in the absence and presence of 25 U/ml SOD. (**G**) H_2O_2 production was assessed in the absence and presence of 100 U/ml catalase. For these experiments, HRP was reduced to 100 mU/ml in order to allow catalase to outcompete HRP for any potential H_2O_2. All data are mean ± SEM, n=3-4/group.

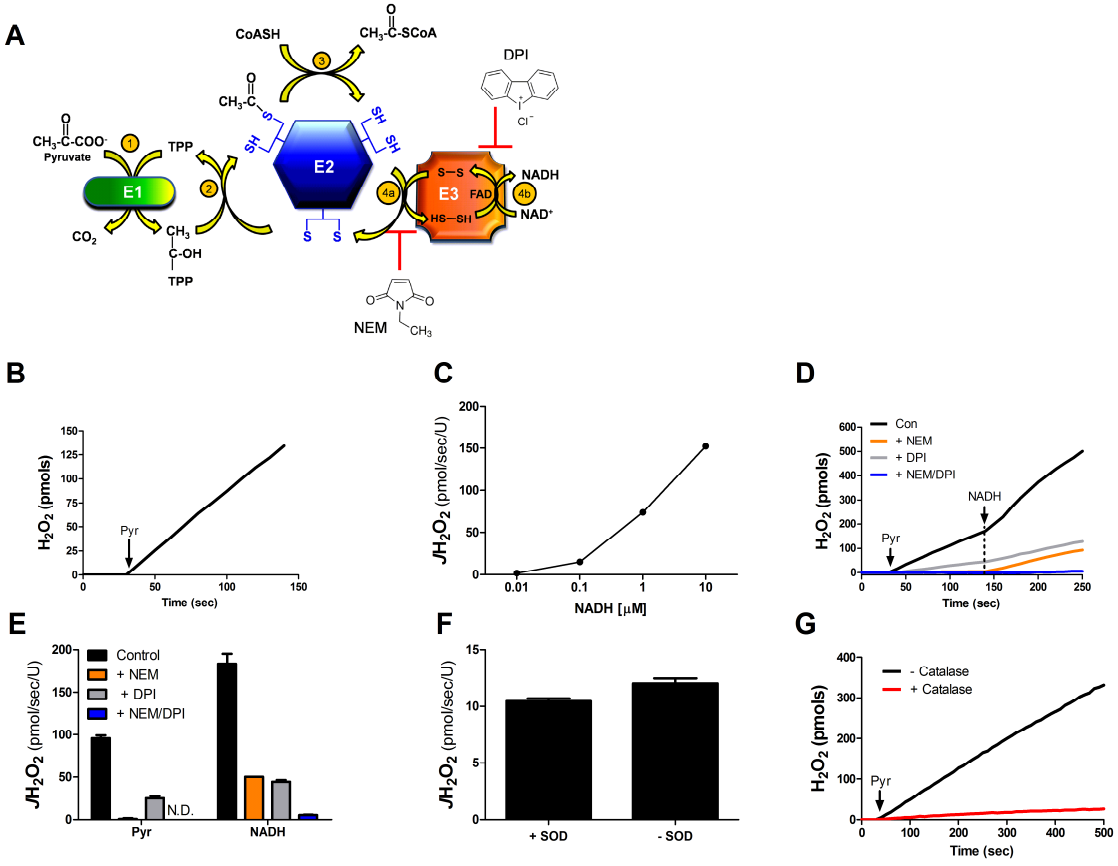

Figure 5. Pyruvate-supported JH_2O_2 from isolated PDH is a function of E2 reducing pressure. H_2O_2 production was assessed in response to increasing concentrations of pyruvate in the absence (**A**) or presence (**B**) of NAD^+. K_m and V_{max} values (with respect to H_2O_2 production) were calculated using Prism statistical software. *Different from - NAD^+ condition. (**C**) H_2O_2 production was assessed in response to increasing concentrations of NAD^+ in the presence of 1 mM pyruvate. NAD^+ concentrations were converted to logarithmic values and an IC_{50} value was obtained. (**D**) Representative H_2O_2 production (red trace) and NADH production (blue trace) experiment in response to 1 mM pyruvate and 5 mM oxaloacetate (50 μM NAD^+ was present for all assays). (**E**) Pyruvate-supported H_2O_2 and NADH production were assessed in the presence of 50 μM NAD^+. JH_2O_2 and JNADH were plotted together (pmol/sec). (**F**) Quantified JH_2O_2 from experiment depicted in panel **D**. In addition to the peak, H_2O_2 production was quantified for the first 30 seconds following pyruvate addition, as well as following OAC administration. *Different from all other conditions ($p < 0.05$). (**G**) Isolated PDH was incubated with recombinant PDK4 protein for 10 minutes at room temperature in the absence or presence of 2 mM ATP. H_2O_2 and NADH production were then assessed. *Different from Con ($p < 0.05$). (**H-I**) Pyruvate supported oxygen consumption (**H**) and H_2O_2 emission (**I**) was assessed in permeabilized fibers prepared from RG $PDK4^{-/-}$ mice and WT (C57BL/6J) controls. *Different from WT mice ($p < 0.05$). Data are mean ± SEM, (**A-G**) n = 3-4/group, (**H-I**) n = 7/group.

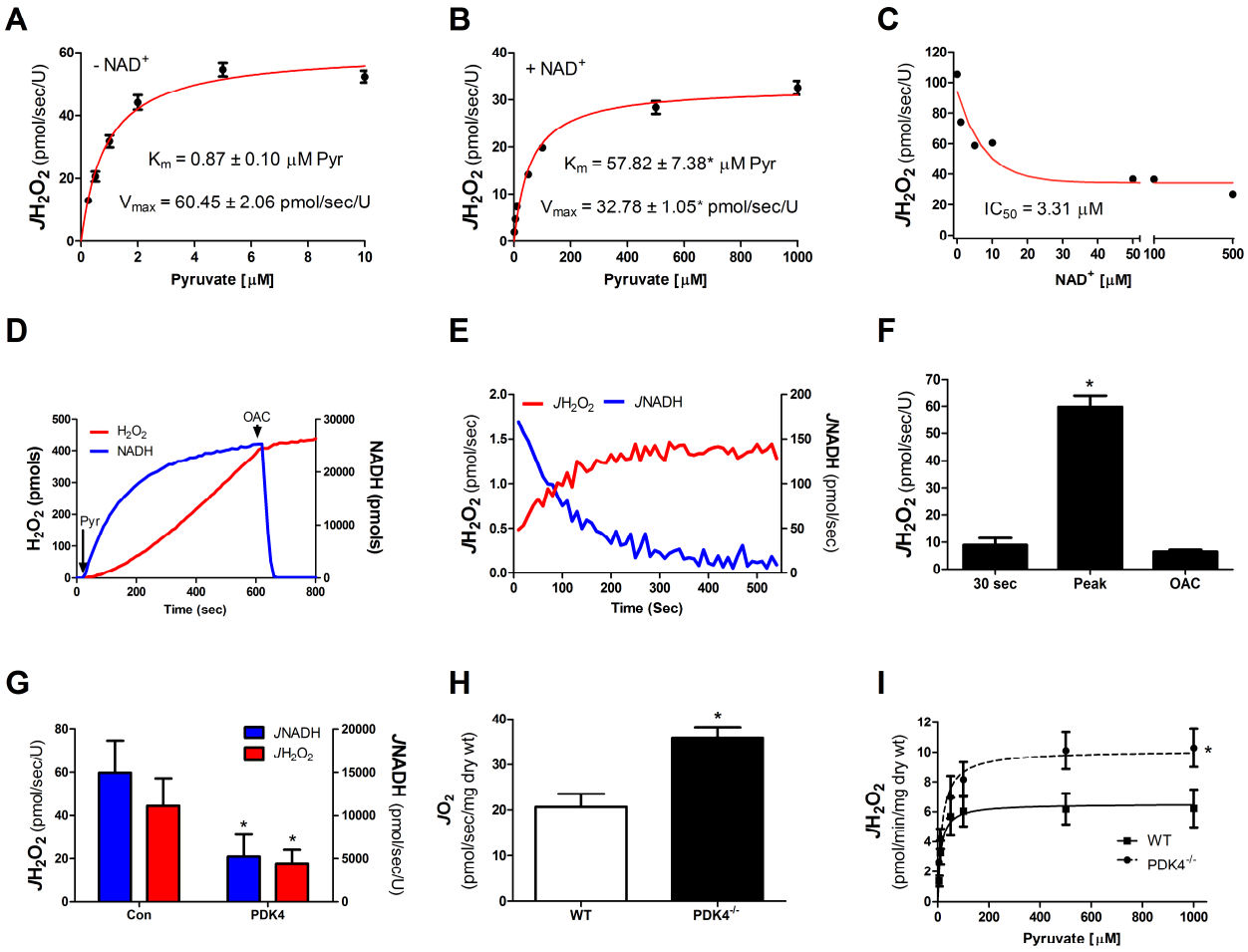
A
- NAD+
Km = 0.87 ± 0.10 μM Pyr
Vmax = 60.45 ± 2.06 pmol/sec/U
JH2O2 (pmol/sec/U)
Pyruvate [μM]
B
+ NAD+
Km = 57.82 ± 7.38* μM Pyr
Vmax = 32.78 ± 1.05* pmol/sec/U
JH2O2 (pmol/sec/U)
Pyruvate [μM]
C
IC50 = 3.31 μM
JH2O2 (pmol/sec/U)
NAD+ [μM]
D
H2O2
NADH
OAC
Pyr
H2O2 (pmols)
NADH (pmols)
Time (sec)
E
JH2O2
JNADH
JH2O2 (pmol/sec)
JNADH (pmol/sec)
Time (Sec)
F
JH2O2 (pmol/sec/U)
30 sec
Peak
OAC
G
JNADH
JH2O2
JH2O2 (pmol/sec/U)
JNADH (pmol/sec/U)
Con
PDK4
H
JO2
(pmol/sec/mg dry wt)
WT
PDK4-/-
I
JH2O2
(pmol/min/mg dry wt)
WT
PDK4-/-
Pyruvate [μM]

Figure 6. Differential effects of carnitine and malate on pyruvate-supported JO_2, JNADH and JH_2O_2. (**A-I**) Permeabilized fibers were prepared from mouse RG. (**A**) JO_2 consumption in response to 1 mM pyruvate and 5 mM carnitine under state 4 conditions. *Different from Pyr ($p < 0.05$). (**B**) Representative NADH production experiment in response to 1 mM pyruvate and 5 mM carnitine. Fibers were pre-incubated in alamethicin (30 µg/ml) prior to assay to permeabilize mitochondria. Numbers above trace represent mean NADH production rates (pmol/sec/mg). (**C**) JH_2O_2 emission in response to 1 mM pyruvate and 5 mM carnitine under state 4 conditions in fibers pre-treated with varying concentrations of CDNB. *Different from Pyr ($p < 0.05$). (**D**) Representative H_2O_2 emission experiment following addition of 1 mM pyruvate and 5 mM carnitine in the presence or absence of BCNU (100 µM) and AF (0.5 µM). (**E**) Quantified JH_2O_2 emission rates from experiment in panel **D**. *Different from – BCNU/AF ($p < 0.05$). (**F-G**) Permeabilized fiber bundles were prepared from RG of $CrAT^{M-/-}$ and their WT littermates (n = 5-6/group). JH_2O_2 emission was assessed in response to 1mM pyruvate and 5 mM carnitine, either in the absence (**F**) or presence (**G**) of BCNU/AF. *Different from WT ($p < 0.05$). (**H-I**) JH_2O_2 emission in response to 1 mM pyruvate and 2 mM malate in the absence (**H**) and presence (**I**) of BCNU/AF. *Different from Pyr condition ($p < 0.05$). Data are mean ± SEM, n = 6-10/group.

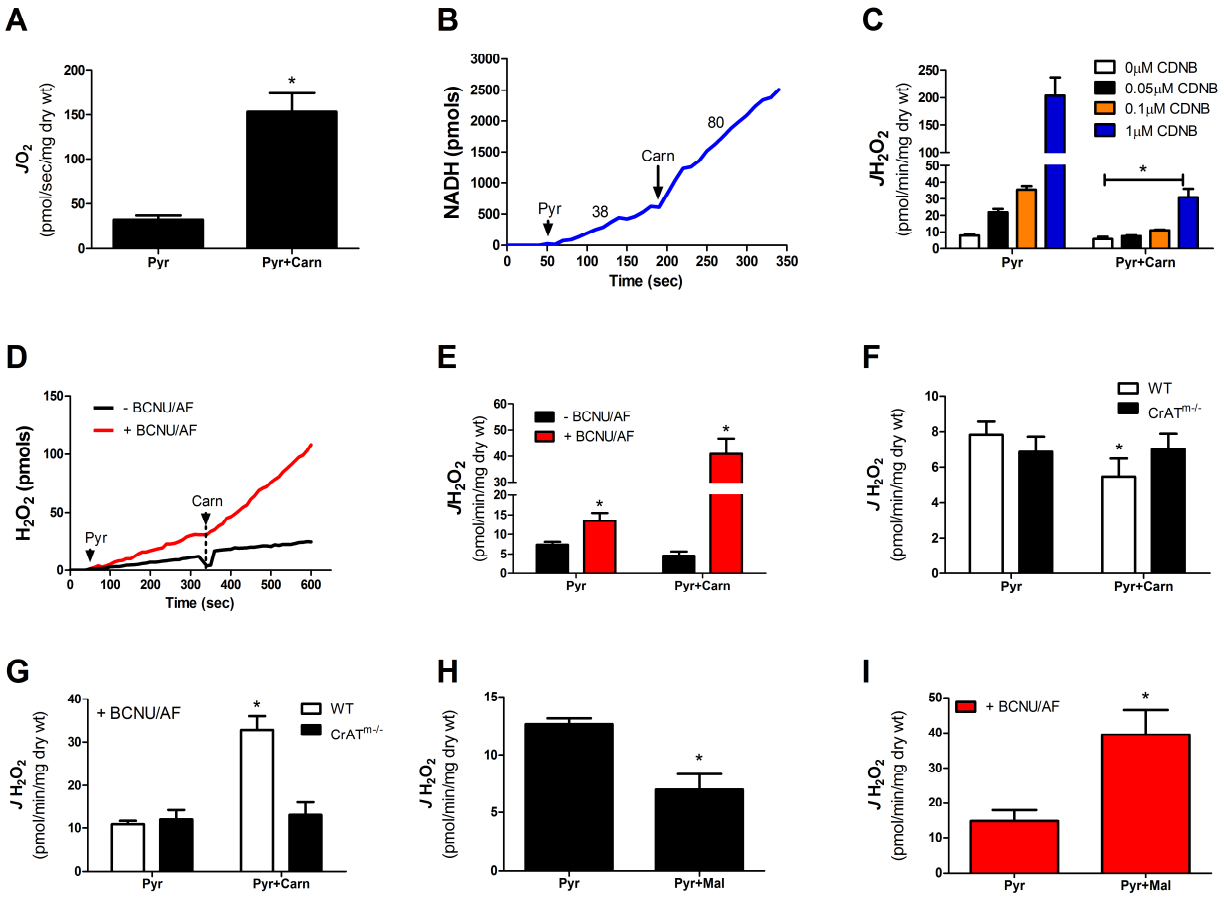

Figure 7. Impact of NNT function/expression on PDH-supported JH_2O_2. Permeabilized fibers were prepared from RG of C57BL/6N (**A-B**) and C57BL/6J (**B-D**) mice. (**A**) JH_2O_2 emission in response to sequential addition of 1 mM pyruvate, 5 µM FCCP and 5 mM carnitine. *Different from Pyr condition ($p < 0.05$). (**B**) Representative H_2O_2 emission experiment following the addition of 1 mM pyruvate and 5 mM carnitine in fibers prepared from C57BL/6N (black trace) and C57Bl/6J (red trace) mice. (**C**) Quantified JH_2O_2 emission rates from experiment in panel **B**. *Different from C57BL/6N ($p < 0.05$). (**D**) JH_2O_2 emission in response to sequential addition of 1 mM pyruvate, 5 mM carnitine, 2 mM malate, and BCNU/AF (100/0.5 µM). *Different from Pyr ($p < 0.05$). Data are mean ± SEM, n = 7/group.

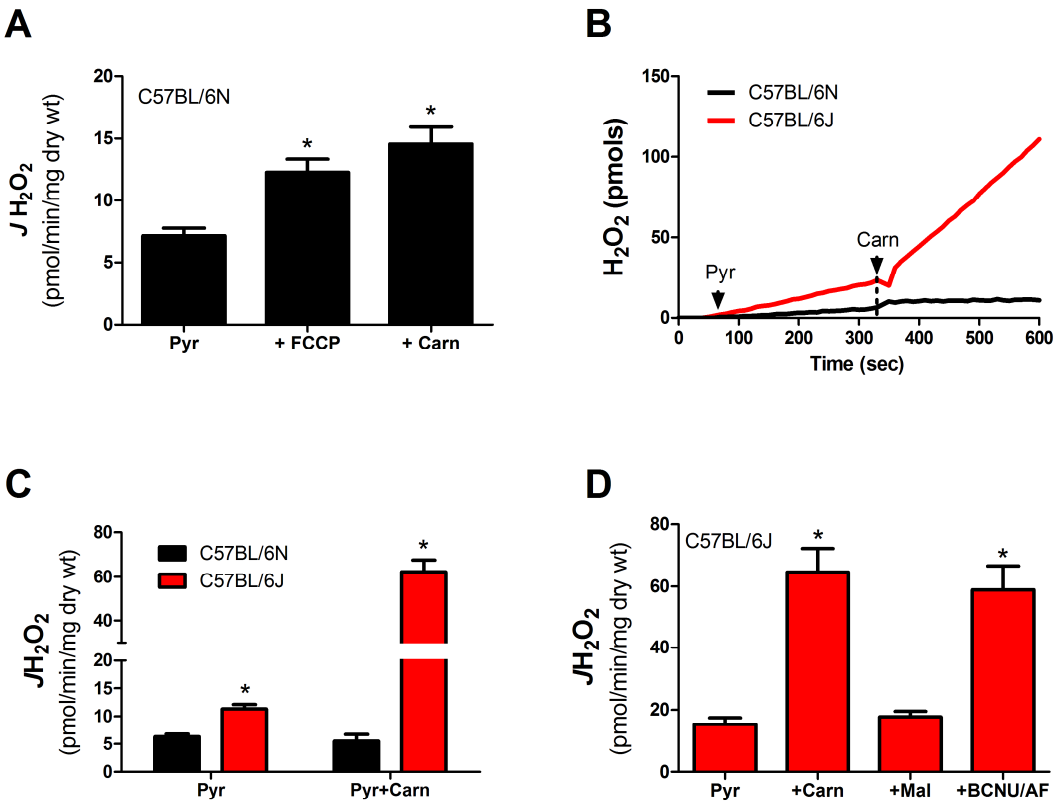

Figure 8. PDH-supported H_2O_2 production under maximal ADP-stimulated conditions. Permeabilized fibers were prepared from RG of C57BL/6J (**A**) and C57BL/6N (**B**) mice. For all experiments, assay buffer was supplemented with hexokinase (1 U/ml) and 2-deoxyglucose (5 mM) to clamp ADP at each desired concentration. (**A**) Pyruvate (1 mM) and carnitine (5 mM)-supported H_2O_2 emission in response to increasing concentrations of ADP (0, 5, 50, 500, 2000 μM). (**B**) JO_2 consumption and JH_2O_2 emission experiments were conducted in response to succinate (10 mM), pyruvate/carnitine (1 mM/5 mM), and glutamate/malate (10 mM/2 mM) in the absence (state 4) and presence (state 3) of maximal ADP (2 mM). Both BCNU (100 μM) and AF (0.5 μM) were present for all assays. Data are presented as the ratio of H_2O_2 produced (pmol/sec/mg) to O_2 consumed (pmol/sec/mg) under state 4 and state 3 conditions. *Different from all other groups under state 4 and state 3 conditions ($p < 0.05$); **Different from G/M under state 4 conditions ($p < 0.05$). Data are mean ± SEM, n = 6-7/group.

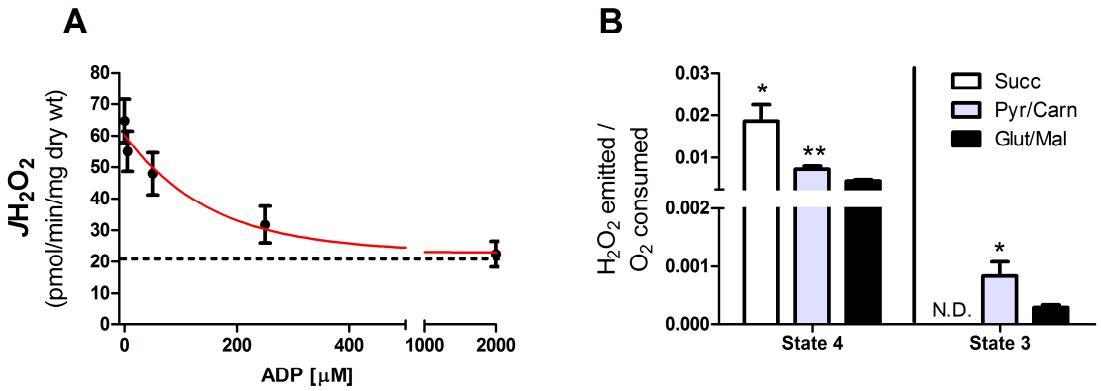

Supplemental Figure 1, Related to Figure 3. CDNB does not impact pyruvate-supported oxygen consumption or NADH production. Permeabilized fiber bundles were prepared from RG of C57BL/6N mice and pre-treated with varying concentrations of CDNB (n = 6/group). (**A**) Oxygen consumption in response to pyruvate 1 mM and carnitine 5 mM under state 4 and state 3 conditions (ADP 2 mM). *Different from 0 µM condition. (**B**) Rate of NADH production in response to pyruvate 1 mM and carnitine 5 mM. Fibers were pre-incubated in alamethicin (30 µg/ml) prior to assay in order to permeabilize mitochondrial membrane. Data are mean ± SEM.

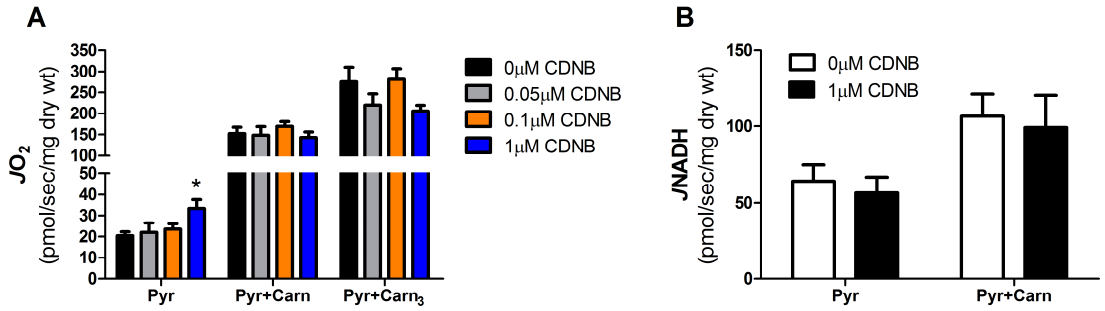

Supplemental Figure 2, Related to Figure 7. Effects of carnitine and malate on pyruvate-supported JO_2 in wild-type and carnitine acetyltransferase (CrAT) knockout mice. (**A**) Permeabilized fiber bundles were prepared from RG of muscle specific CrAT knockout mice ($CrAT^{m-/-}$) and their WT littermates (n = 5-6/group). Oxygen consumption was assessed in response to pyruvate 1 mM and carnitine 5 mM. *Different from WT ($p < 0.05$). (**B**) Permeabilized fiber bundles were prepared from RG of C57BL/6N mice (n = 4/group). Oxygen consumption was assessed in response to pyruvate 1 mM and malate 2 mM under state 4 conditions. *Different from Pyr condition ($p < 0.05$). Data are mean ± SEM.

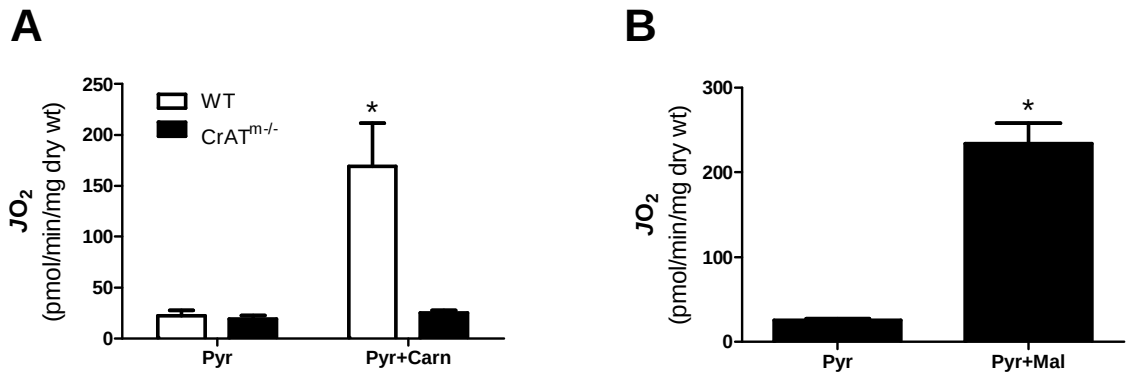

Supplemental Figure 3, Related to Experimental Procedures. (**A**) Representative trace of an H_2O_2 standard curve experiment. Black arrows indicate the addition of H_2O_2. It is critical to understand that the background fluorescence using the Amplex Ultra Red/HRP detection system increases over time, as all experiments are run at 37˚C. To control for this, fluorescence is monitored for a period of ~8-10 minutes during each experiment prior to H_2O_2/substrate addition in order to quantify this background rate (extrapolated background fluorescence is depicted by the dotted line). This background rate of fluorescence is then subtracted from each resorufin trace prior to slope and Y-intercept calculation (for standard curve experiments) or conversion to nM H_2O_2 (H_2O_2 emission experiments). (**B**) Representative H_2O_2 standard curve. (**C**) Quantified slopes (resorufin A.U./H_2O_2) from H_2O_2 standard curve experiments performed in the presence of various substrates. *Different from vehicle control ($p < 0.05$). Data are mean ± SEM. (**D**) Representative traces of resorufin fluorescence in the presence of increasing concentrations of NADH. Black arrows indicate μM additions of NADH.

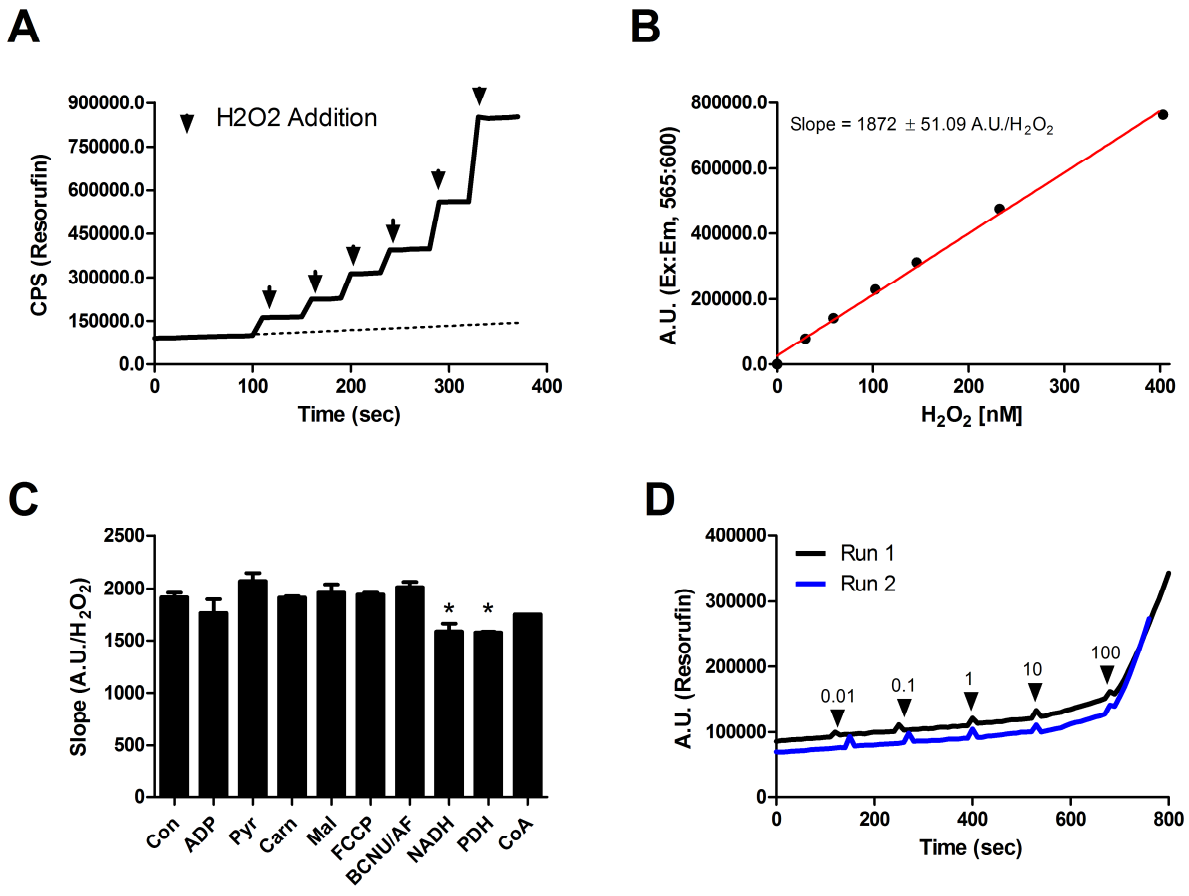

CHAPTER 3: LOSS OF FUNCTIONAL NICOTINAMIDE NUCLEOTIDE TRANSHYDROGENASE IN C57BL/6J MICE COMPROMISES SKELETAL MUSCLE REDOX BUFFERING CAPACITY AND ALTERS WHOLE BODY ENERGY METABOLISM

Abstract

Nicotinamide nucleotide transhydrogenase (NNT) utilizes mitochondrial membrane potential to drive the thermodynamically unfavorable reduction of $NADP^+$ from NADH. NADPH, once produced, then provides reducing power for the principle redox buffering networks (glutathione and thioredoxin) operating within the matrix. C57BL/6J mice are deficient in NNT due to a naturally occurring in-frame five exon deletion within the gene encoding NNT. These mice are characterized by an increased susceptibility to develop obesity, insulin resistance and type II diabetes when placed on a HFD. The present study was undertaken to determine the potential consequences of NNT loss within these mice on skeletal muscle mitochondrial function. Results contained herein demonstrate a clear role for NNT in contributing to skeletal muscle mitochondrial redox buffering integrity as well as whole body-energy metabolism. These findings help to explain the increased susceptibility to obesity and insulin resistance previously observed in the C57BL/6J strain and are the first to demonstrate a role for NNT in contributing to whole body energetic demand.

Introduction

C57BL/6J mice are one of the most routinely employed animal models of glucose metabolism within the field of diabetes research. These mice display symptoms of

glucose intolerance as early as 6 weeks of age (30) and are highly susceptible to the development of obesity, insulin resistance and overt type II diabetes when placed on a high fat diet (HFD) (30, 55, 56). In an elegant series of experiments conducted by Toye et al., (57) the phenotype of the C57BL/6J strain was mapped to a naturally occurring in-frame five exon deletion within the nicotinamide nucleotide transhydrogenase (NNT) gene, which removes exons 7-11 of the mature peptide, effectively creating an NNT whole body knockout (16, 23). This mutation is believed to have occurred sometime between 1970 and 1984 and is apparently specific to the pure C57BL/6J strain produced only by the Jackson Laboratory (http://jaxmice.jax.org/strain/000664.html). Follow up experiments in which functional NNT was reintroduced via transgenic expression successfully rescued the impaired insulin secretion and glucose intolerant phenotype of the C57BL/6J mice (16). A role for NNT in controlling pancreatic insulin secretion was subsequently demonstrated using siRNA directed at the protein within an insulin secreting cell line (15). With regards to the mechanism of action, loss of NNT is believed to elevate mitochondrial peroxide exposure within the beta cell in response to glucose uptake, thereby lowering the ATP:ADP ratio (through an as yet unidentified mechanism), delaying closure of the K_{ATP} channel and ultimately impairing first-phase insulin secretion (15, 46). While the impact of NNT loss on insulin secretion within the C57BL/6J strain has been thoroughly investigated, very little is currently known about the effects of this mutation on other tissues, specifically within insulin sensitive peripheral tissues (e.g., skeletal muscle).

NNT, along with NADP-linked isocitrate dehydrogenase and decarboxylating malate dehydrogenase (malic enzyme; also present in the cytosol) are responsible for

maintaining mitochondrial reducing power in the form of NADPH/$NADP^+$. NNT is particularly interesting in that it has been shown to account for approximately 50% of matrix NADPH (46) and exists as a proton-translocating enzyme that utilizes the electrochemical proton motive force (Δp) generated by the respiratory complexes to drive the thermodynamically unfavorable reduction of $NADP^+$ from NADH (21). Much of the literature thus far investigating the pathophysiological consequences of altered cell redox (i.e., "oxidative stress") has primarily focused on the deleterious impact of elevated peroxide production in terms of disease etiology. However; based on the current working model of the organization/structural characteristics of redox signaling networks, protein redox status is primarily dictated not by H_2O_2 production, but rather by supply of reducing power (i.e., NADPH) (17). That is, alterations in cellular redox could just as easily be propagated via a reduction in NADPH supply as they could by an increase in H_2O_2 production. This concept represents a potential paradigm shift within the field in which investigative emphasis is directed not only towards uncovering the specific proteins responsible for H_2O_2 generation, but also to those tasked with the maintenance of cellular reducing power (i.e., NADPH producing enzymes). To this end, NNT represents an intriguing target of investigation given its overall contribution to matrix NADPH and dependence on mitochondrial energization. The present study was undertaken to determine the potential consequences of NNT loss on skeletal muscle mitochondrial redox status and respiratory function, as well as whole body energy metabolism. Results contained herein demonstrate a clear role for NNT in controlling mitochondrial peroxide emission, particularly that arising from the pyruvate dehydrogenase complex (PDH). In addition, a role for NNT in contributing to energetic

demand is demonstrated both at the mitochondrial level using a TPP^+ selective electrode to assess mitochondrial membrane potential, as well as at the whole body level via indirect calorimetry. With respect to the latter, C57BL/6J mice were found to consume less oxygen and thus have lower energy expenditure per gram of lean mass compared to C57BL/6N mice which express functional NNT. These findings are the first to demonstrate a role for NNT in regulating both skeletal muscle redox homeostasis and whole body energy metabolism, both of which may contribute to the well characterized glucose intolerant and obesity prone phenotype of the C57BL/6J strain.

Results

Assessment of glucose tolerance and insulin sensitivity within C57BL/6N (6N) and C57BL/6J (6J) mice.

Consistent with previous reports demonstrating impaired glucose tolerance in C57BL/6J mice (30, 57), area under the curve (AUC) for blood glucose during an IPGTT was greater in the 6J mice at ~ 10 weeks of age (Figure 9A & 9B). Fasting blood glucose however was not different (*6N* 160.6 ± 14.6; *6J* 165.6 ± 11.3 mg/dl). Both AUC for blood glucose during an ITT (Figure 9C) and ex vivo insulin-stimulated glucose uptake (Figure 9D) were not different, thus suggesting similar levels of insulin sensitivity between strains.

Assessment of whole-body energy metabolism reveals stark differences in energy expenditure between strains

Assessment of terminal body composition revealed ~ 2 fold greater fat mass in 6J compared to 6N mice, despite no differences in lean or total body mass (Figure 9E).

These findings are in agreement with previous reports (41, 54) and provide evidence of differences in whole-body energy metabolism between strains. To directly address this question, a separate cohort of 6N and 6J mice were placed inside indirect calorimetry units in which rates of oxygen consumption and carbon dioxide production were continuously monitored along with ambulatory activity and food/water intake for a period of 5 days. Analysis revealed clear reductions in oxygen consumption (Figure 10A & 10D), carbon dioxide production (Figure 10B & 10E) as well as calculated energy expenditure (Figure 10C & 10F) in the 6J mice. These differences were apparent whether the data were normalized to fat free mass (Figure 10A-C) or total body mass (Figure 10D-F) and could not be explained by differences in RER (Figure 10G), food intake (Figure 10H) or ambulatory activity (Figure 10I). The fact that normalization to fat free mass did not eliminate the apparent differences in energy metabolism suggested that the reduced oxygen consumption and energy expenditure observed in the 6J mice may be related to inherent differences in skeletal muscle metabolism, as skeletal muscle accounts for approximately ~ 40% of total body mass and ~ 30% of resting energy expenditure (62).

No evidence of reduced mitochondrial content in C57BL/6J mice

To determine if strain differences in whole-body oxygen consumption may be related to mitochondrial content and/or functional capacity, protein abundance and respiratory capacity were assessed in skeletal muscle. Assessment of protein content via immunoblot revealed no differences between strains for any of the respiratory complexes (Figure 11A). As an index of functional capacity, maximal uncoupled respiration was assessed in permeabilized fibers prepared from red gastrocnemius

muscle under saturating substrate (10 mM glutamate, 2 mM malate, 2 mM ADP, 10 mM succinate, and 500 nM FCCP) conditions. These experiments revealed no differences in respiratory capacity between strains (Figure 11B). Collectively, these data do not support a role for reduced mitochondrial content and/or functional capacity in contributing to the altered energy metabolism observed in the 6J mice.

Loss of functional NNT compromises pyruvate-supported JO_2 consumption and elevates mitochondrial membrane potential (ΔΨ)

While knockout of NNT in Caenorhabditis elegans (5), as well as PC12 cells (60) has indeed been shown to impair cellular redox homeostasis (oxidative shift in the glutathione pool), as well as increase sensitivity to peroxide exposure, and alter energy metabolism (reduced respiration and levels of ATP), very little is currently known as to how loss of this protein may affect skeletal muscle mitochondrial function. Given that NNT accounts for ~50% of matrix NADPH, coupled with the dependence of NNT function on mitochondrial membrane potential, it was hypothesized that loss of this protein may have far reaching consequences on mitochondrial function under substrate combinations designed to maximize NNT activity. To test this hypothesis, JO_2 consumption and mitochondrial membrane potential (ΔΨ) were assessed in permeabilized fibers in the presence of pyruvate and carnitine or succinate alone. The combination of pyruvate and carnitine provides a unique situation in which the pyruvate dehydrogenase complex (PDH) and NNT exist as the sole sources of NADH and NADPH, respectively. Under these conditions, respiration rate was lower in fibers prepared from 6J mice both in the absence (state 4) and presence (state 3) of ADP (Figure 12A). Mitochondrial membrane potential (ΔΨ) was not different under state 4

conditions (despite lower JO_2 consumption in the 6Js), but was slightly more negative in the 6J mice upon transition to state 3 respiration (Figure 12B & 12D). While the slightly more negative ΔΨ in the 6J mice (6N -137.0 mV; 6J -143.7 mV) suggests a role for NNT in contributing to metabolic demand (i.e., Δp consumption), these data do not rule out the possibility of potential oxidative modification made to PDH or the respiratory system as a consequence of reduced NADPH-dependent peroxide buffering. To test this possibility, pyruvate/carnitine JO_2 consumption experiments were repeated in the absence and presence of the thiol reducing agent dithiothreitol (DTT). The addition of DTT completely normalized respiration rates between strains (Figure 12C), thus suggesting a role for H_2O_2-mediated oxidative modifications in contributing to the respiration impairments observed in the 6J mice.

Similar to pyruvate/carnitine, the provision of succinate as the sole substrate restricts NADPH supply to the level of NNT, with the exception of a small contribution from malic enzyme following succinate oxidation (succinate → fumarate → malate). Under these conditions, reverse electron flow from complex II back to complex I results in the reduction of NAD^+ to NADH, which can subsequently be utilized by NNT to provide NADPH at the expense of ΔΨ. In contrast to that observed for pyruvate/carnitine, succinate supported respiration was not found to differ between strains under state 4 conditions (Figure 12E). However, assessment of succinate-supported ΔΨ revealed a significantly more negative membrane potential in fibers prepared from 6J mice (6N -194.5 mV; 6J -204.8 mV) (Figure 12F). Taken together, these data support a role for NNT in contributing to metabolic demand under substrate conditions which rely on NNT as the principle source of NADPH. Moreover, elevations in ΔΨ coupled with apparent

reductions in peroxide-buffering capacity (evidenced by the DTT experiment) within the 6J mice suggest the presence of severely elevated H_2O_2 emitting potential.

Pyruvate and succinate-supported H2O2 emission are elevated in C57BL/6J mice.

As anticipated, assessment of JH_2O_2 emitting potential in permeabilized fibers prepared from 6N and 6J mice revealed ~ 2 fold greater emission rates in the 6J mice in response to pyruvate (Figure 13A). In order to determine the impact of NNT on pyruvate alone-supported JH_2O_2 emission, NNT activity was inhibited using the chemical uncoupler FCCP. Addition of FCCP following pyruvate increased JH_2O_2 emission in the 6N mice to the level of the 6Js (Figure 13B), suggesting a role for NNT in regulating peroxide emission from NADH-linked dehydrogenases such as PDH. Assessment of JH_2O_2 emission in the presence of pyruvate and carnitine revealed drastic differences between strains (Figure 13C). Compared to pyruvate-alone supported JH_2O_2 emission, the inclusion of carnitine increased JH_2O_2 emission in the 6J mice approximately 5 fold, while decreasing emission within the 6Ns (compare Pyr rates from Figure 13B to Pyr/Carn rates in Figure 13D). As an aside, the divergent response to carnitine between the two strains is observed without exception, and as such can be used as a surrogate means of genotyping unknown strains of mice as either 6N or 6J. To determine the influence of NNT on pyruvate/carnitine supported JH_2O_2 emission, NADPH-dependent reductase activity (both glutathione and thioredoxin) was inhibited via bis-chloroethylnitrosourea (BCNU) and auranofin (AF). In the presence of BCNU/AF, pyruvate/carnitine supported JH_2O_2 emission was unchanged in 6J mice and starkly elevated within the 6N mice, albeit not to the level of the 6Js (Figure 13C & 13D). Investigation into the individual contribution of glutathione reductase (GR) and

thioredoxin reductase (TrxR) to the control of pyruvate/carnitine supported JH_2O_2 emission, revealed a greater contribution from TrxR (Figure 13E & 13F). Pyruvate supported JH_2O_2 emission in the presence of malate was also elevated in the 6J mice; however, the addition of BCNU/AF completely normalized emission rates between groups (Figure 13G & 13H). The lower emission rates in the presence of malate (compare Pyr rates from Figure 13B to Pyr/Mal rates in Figure 13H) are reflective of the ability of malate to supply reducing power (i.e., NADPH) independent of NNT activity via isocitrate dehydrogenase and malic enzyme.

Consistent with that observed in the presence of pyruvate, succinate supported JH_2O_2 emission was elevated ~ 2 fold in the 6J mice (Figure 14A). The addition of BCNU and AF under succinate-energized conditions increased JH_2O_2 emission in both 6N and 6J mice, with the effect being much more pronounced in the former (Figure 14B & 14C). Emission rates in the presence of BCNU/AF were not found to be statistically different between strains. Despite the stark differences in H_2O_2 emitting potential between strains, assessment of glutathione redox status within skeletal muscle homogenate from both soleus and tibialis anterior muscle revealed no differences (Figure 15A & 15B). The lack of apparent oxidation within the glutathione pool may reflect the experimentally determined less dominant role of glutathione reductase in controlling peroxide emission compared to TrxR (Figure 13E &13F). Alterations in thioredoxin redox status may have revealed strain differences; however, assessment of Trx redox state within tissue homogenate has several limitations and thus was not performed in the present study.

Discussion

The NNT-deficient C57BL/6J strain is a particularly useful model for the study of metabolic disease in that they possess a unique susceptibility to develop obesity, insulin resistance and type II diabetes when fed a HFD (30, 54, 55). While impairments in first-phase insulin secretion have been identified as the principle factor responsible for the glucose intolerant phenotype of the C57BL/6J line (15), these defects do not explain the propensity for body fat accumulation and/or peripheral insulin resistance also observed in these mice. Given the growing body of literature suggestive of a "causal" role for altered cellular redox status in the development of insulin resistance (2, 22) in conjunction with the importance of NNT in maintaining redox homeostasis (5, 60), it was hypothesized that loss of NNT within C57BL/6J mice may have additional impacts particularly within skeletal muscle mitochondria which may contribute to their increased propensity for metabolic disease. In this context, there are three main findings from the present study. First, NNT was shown to be a critical component of the mitochondrial redox buffering network operating within skeletal muscle. Loss of this function in C57BL/6J mice was shown to severely elevate mitochondrial H_2O_2 emitting potential as well as disrupt pyruvate supported respiratory kinetics. Second, NNT deficiency was found to generate a more negative $\Delta\Psi$ in the presence of pyruvate/carnitine/ADP and succinate. To our knowledge, this is the first evidence portraying a role for NNT in the dissipation of Δp under physiological constraints. Lastly, lack of NNT in C57BL/6J mice was shown to result in reduced whole body oxygen consumption and energy expenditure compared to C57BL/6N mice, despite similar levels of activity and food intake. Collectively, the present findings expand the function of NNT beyond the level of

an NADPH-generating enzyme and establish the protein as a critical regulator of both matrix redox buffering capacity and energetic demand.

The mitochondrial respiratory system is comprised of several multi-polypeptide protein complexes embedded within the inner mitochondrial membrane. Electrons derived from the oxidation of carbon-based substrates are transferred through a series of redox couples within these complexes with O_2 serving as the final electron acceptor, ultimately reducing $½O_2$ to H_2O (13). Energy released during electron transfer is harnessed at three locations within the respiratory system to drive the translocation of protons from the matrix to the inner membrane space. This creates a proton gradient across the inner membrane that is derived from both the concentration and the electrical potential difference across the membrane, collectively referred to as the proton motive force (Δp). The electrical-chemical potential energy created by the generation of Δp is sufficient to drive the synthesis of ATP as protons flow back through the ATP synthase complex into the matrix. While ATP synthase is the principle consumer of Δp, a variety of other energy-dependent cellular processes are dependent upon Δp within the matrix. These include, adenine nucleotide translocase (ANT), calcium uptake, substrate transport and NNT activity. These energy-consuming processes combine to determine the energetic demand within the system at any point in time. A key point to emphasize is that both the generation and dissipation of Δp is a “demand” driven process. That is, the oxidation of substrate and subsequent flux of electrons throughout the respiratory system is determined by the rate of Δp consumption. From a whole organism perspective, a greater rate of oxygen consumption corresponds to a greater rate of Δp consumption (i.e., high demand), whereas reduced oxygen consumption reflects a slower rate of Δp

consumption (i.e., low demand). In the present study, C57BL/6J mice, which lack functional NNT and thus lack any potential contribution by the enzyme to Δp dissipation, were found to have lower whole body oxygen consumption per gram of fat free mass. These data provide rather compelling evidence for a role of NNT in contributing to whole body energy expenditure and thus may explain the previously reported increased susceptibility to diet-induced obesity in C57BL/6J mice (41, 54), as well as the increased adiposity observed herein.

In addition to whole-body adiposity, mitochondrial electron leak and subsequent formation of $O_2\bullet^-/H_2O_2$ is also highly sensitive to metabolic demand. Periods of increased nutrient delivery (i.e., ↑NADH/NAD^+) in the face of low energetic demand (i.e., ↓ Δp consumption) elevate reducing pressure within the respiratory system as well certain H_2O_2 generating dehydrogenases (e.g., PDH, KGDH), and have been shown to promote maximal rates of electron leak (34, 37, 38, 53). This increase in propensity for electron leak in response to nutrient overload has been suggested to play a causal role in the development of high fat diet-induced insulin resistance (2, 20, 22). In response to high fat feeding, an increased burden is immediately placed upon the redox buffering systems operating within the matrix to both attenuate excessive peroxide emission and prevent aberrant oxidation within the redox-sensitive proteome. Evidence in support of this notion is supplied by several investigations in which supplementation of the redox buffering network via mitochondrial targeted transgenic and/or pharmacological interventions has been shown to protect against the onset of diet-induced insulin resistance (2, 11, 20). Based on this concept, it is hypothesized that the clear reductions in redox buffering capacity observed in the present study within the

C57BL/6J mice may contribute to their increased susceptibility to develop insulin resistance when fed a HFD. More to the point, loss of NNT would be expected to be particularly detrimental given its role in contributing not only to NADPH generation but also to Δp dissipation; a function which serves to attenuate reducing pressure and electron leak throughout the system.

In aggregate, the present study sheds valuable insight into a role for NNT in contributing to skeletal muscle mitochondrial redox buffering integrity as well as whole body-energy metabolism. These findings help to explain the increased susceptibility to obesity and insulin resistance previously observed in the C57BL/6J strain and are the first to demonstrate a role for NNT in contributing to whole body energetic demand. Future investigation is required in order to determine if indeed alterations in NNT activity/expression are involved in the etiology of metabolic disease.

Experimental Procedures

Animals and Reagents

All animal studies were approved by the East Carolina University Institutional Animal Care and Use Committee. C57BL/6NJ (6N) and C57BL/6J (6J) mice were purchased from Jackson Laboratory. All mice were housed in a temperature (22˚C) and light controlled (12 hour light/12 hour dark) room and maintained on 10% low fat diet with free access to food and water. For all experiments, mice were fasted 4 hours, anesthetized, and red portions of the gastrocnemius muscle were dissected and separated into fiber bundles. Remaining portions of muscle were frozen (liquid N_2) for later analysis. All reagents and chemicals were obtained from Sigma-Aldrich with the

exception of Amplex Ultra Red reagent (Invitrogen), GSH/GSSG assay kit (Oxis International Inc.), and Total OXPHOS Rodent WB Antibody Cocktail (Mitosciences).

Glucose and Insulin tolerance testing

All experiments were performed following a 4 hour fast at approximately 12:00pm. Blood glucose was monitored using the Blood Glucose Alpha Track Monitoring System from samples collected at the distal tail vein. Following an initial blood glucose measurement, glucose (2g/kg FFM) or insulin (0.5U/kg FFM) was injected intraperitoneally and glucose measurements were made every 10-20 minutes for a period of 90-120 minutes.

$^{3+}$H-2-Deoxyglucose uptake

Immediately after removal, extensor digitorum longus muscles were placed inside pre-filled wells containing Krebs-Henseleit buffer (KHB) plus 1mM pyruvate with continuous bubbling of 95% O_2-5% CO_2 inside a temperature (37˚C) controlled water bath. Following a 20 min pre-incubation period, muscles were transferred to fresh wells which did or did not contain insulin (50 mU/ml) for 30 min. Muscles were then transferred to incubation wells containing 5mM 2-deoxyglucose (2-DOG), 10mM Mannitol, 0.2µCi/ml $^{3+}$H-2DOG, 0.01µCi/ml ^{14}C-D-Mannitol, and with or without insulin (50 mU/ml). After incubation, muscles were transferred to ice-cold KHB to stop reaction, trimmed of connective tissue and flash frozen until time of analysis. Frozen muscles were weighed and solubilized in 0.1 ml of 0.5N NaOH. Solubilized muscles and incubation media samples were counted in a Beckman LS 5000 TD liquid

scintillation counter preset to count ^{14}C and ^{3}H channels simultaneously. Data are expressed as µmol/g/hr.

Determination of body composition

Measurements of fat and lean body mass were determined using the EchoMRI-500 (Houston, TX) in accordance with the manufacturer's instructions.

Assessment of whole-body energy metabolism

The TSE LabMaster System (TSE Systems, Chesterfield, MO) was used to determine rates of oxygen consumption (VO_2) and carbon dioxide production (VCO_2), respiratory exchange ratio, food and water intake, and energy expenditure. Rates are expressed per g of fat free mass (FFM) or body weight (BW). Infrared sensors were used to record ambulatory activity in three-dimensional axes (X, Y, Z). Counts across all three axes were summed to give total ambulatory activity. All reported measurements represent the average of at least two 12 hour light or dark cycles.

Preparation of permeabilized fiber bundles

This technique is partially adapted from previous methods and has been thoroughly described (44). Following permeabilization, fibers were washed in ice-cold buffer Z (K-MES [110 mM], KCl [35 mM], EGTA [1 mM], K_2HPO_4 [5 mM], $MgCl_2$-6H2O [3 mM], BSA [0.5 mg/ml] pH 7.1, 295 mOsm) to remove endogenous substrates.

Mitochondrial respiration and H_2O_2 emission measurements

High-resolution O_2 consumption measurements were conducted at 37˚C in buffer Z, supplemented with creatine monohydrate (25mM), using the OROBOROS O_2K Oxygraph. Mitochondrial H_2O_2 emission was measured fluorometrically at 37˚C via Amplex Ultra Red (10 μM) / horseradish peroxidase (3 U/ml) detection system (Ex:Em 565:600). Fluorescence was monitored using a SPEX Fluoromax 3 (HORIBA Jobin Yvon) spectrofluorometer with temperature control and magnetic stirring. For each experiment, resorufin fluorescence was converted to nM H_2O_2 via an H_2O_2 standard curve generated under identical substrate conditions (with the exception of a permeabilized fiber) as employed for each protocol. To this end, all substrates utilized were tested for any potential interference with the Amplex Ultra Red/HRP detection system. Blebbistatin (25 μM) was present during all O_2 consumption and H_2O_2 emission experiments to prevent contraction (44). At the conclusion of each experiment, fiber bundles were washed in double-distilled H_2O to remove salts and freeze-dried in a lyophilizer (Lab-conco). The rate of respiration was expressed as pmol/s/mg dry weight and H_2O_2 emission as pmol/min/mg dry weight.

Mitochondrial Membrane Potential (ΔΨ)

ΔΨ and respiration rates of PmFBs were measured simultaneously using the OROBOROS Oxygraph-2k (Oroboros Instruments) combined with electrodes sensitive to TPP^+ (tetraphenylphosponium, a membrane-potential dependent probe) and oxygen at 25°C. All experiments were run in Buffer Z containing 20 mM creatine monohydrate and 25 μM blebbistatin. Individual protocols included: (1) (in mM) 2 malate, 10 glutamate, 15 pyruvate, 10 succinate, 10 glycerol-3-phosphate, 5 2-deoxyglucose, 2

U/mL hexokinase + ADP titration (25, 50, 100, 250, 500, 1000, 2000 µM) + 2 µM FCCP; (2) (in mM) 2 malate, 10 glutamate, 15 pyruvate + 10 succinate + 2 ADP + 2 µM FCCP. For each protocol the TPP^+ electrode was calibrated by a 5 point titration (1.1-1.5 µM TPP^+) for quantifying the concentration of TPP^+.

The calculation of ΔΨ is based on the Nernst equation with binding correction factors and estimated mitochondrial protein content to PmFB freeze-dried weight. The Oroboros TPP^+- ΔΨ calculation template (www.oroboros.at) was used with the following equation:

$$\Delta\Psi = \frac{RT}{zF} \cdot \ln\left(\frac{\frac{n_{add}}{c_{ext,free}} - V_{ext} - K_O' \cdot P_C}{V_{mt}(spec) \cdot P_{mt} + K_i' \cdot P_{mt}} \right)$$

Variables and constants of the equation include: n_{add} = total amount of ions added to system; $c_{ext,free}$ = free concentration of probe ion outside mitochondria; V_{ext} = volume of external solution outside mitochondria; V_{mt} = volume of mitochondrial matrix (1 µl/mg (35)); K_i' = internal partition coefficient of TPP^+ (7.9 µl/mg (35)); K_o' = external partition coefficient of TPP^+ (14.3 µl/mg (35)); P_{mt} = total mitochondria protein content (7.5% of mg dry weight) (24, 42); P_c = total cellular protein content (equivalent to PmFB mg dry weight).

Western blot analysis

Frozen muscles were homogenized in TE buffer (10 mM Tris, 1 mM EDTA), supplemented with an anti-protease cocktail (Sigma) and combined 1:1 with Laemmli Sample Buffer (Bio-Rad), which contained 10 mM dithiothreitol (DTT). Proteins were

separated by SDS-PAGE and electrotransferred to polyvinylidene fluoride (PVDF) membranes (Millipore, Billerica, MA). Membranes were blocked for 1 hour at room temperature using Odyssey Blocking Buffer (LI-COR Biosciences) and then probed overnight (4˚C) with a Total OXPHOS Rodent WB Antibody Cocktail (1:1000) (Mitosciences). Following washing, membranes were incubated for 1h at room temperature with a mouse secondary antibody and the immunoreactive proteins were detected using the Odyssey infrared imagining system. Results were normalized for total protein using MemCode Reversible Protein Stain (Pierce, Rockford, IL).

GSH, GSSG, GSH/GSSG measurements

Frozen muscles were homogenized in TE buffer (10 mM Tris, 1 mM EDTA) that was pre-bubbled with N_2 gas for ~20 minutes prior to homogenization. Bubbling of N_2 gas prior to homogenization was found to be critical in preventing ex-vivo oxidation of the glutathione pool. Immediately following homogenization, a portion of homogenate was transferred to a separate tube containing 0.5 mM 1-methyl-2-vinylpyridinium triflate (M2VP), which was utilized to assess GSSG. Samples were spun down (10,000 RPM, 4˚C) and supernatant was utilized to measure GSH and GSSG using the reagents and calibration set provided by the GSH/GSSG assay kit (Percipio Biosciences).

Statistics

Data are presented as mean ± SEM. Statistical analysis were performed using t-tests or 1-way ANOVA with Student-Newman-Keuls methods for analysis of significance among groups. The level of significance was set at $P < 0.05$.

ACKNOWLEDGEMENTS

This work was supported by funding from the NIH; 1F32AR061946 (LAAG),

1R01DK089312 (D.M.M.), 1R01DK074825 and 1R01096907 (P.D.N.).

Figure 9. Differences in glucose tolerance and terminal body composition between C57BL/6N and C57BL/6J mice. (A) Intraperitoneal glucose (2g/kg FFM) tolerance tests were performed at ~10-12 weeks of age. (**B**) Area under the curve (AUC) was calculated using Prism statistical software. (**C**) Intraperitoneal insulin (0.5U/kg FFM) tolerance tests were performed at ~10-12 weeks of age. (**D**) Basal and insulin (50mU/ml) stimulated ^{3}H-2-deoxyglucose uptake was assessed in EDL muscle at ~12-14 weeks of age. (**E**) Fat and lean body mass were determined using the EchoMRI-500 (Houston, TX) at ~10-12 weeks of age. *Different from Pyr condition ($p < 0.05$). Data are mean ± SEM, n = 9-10/group.

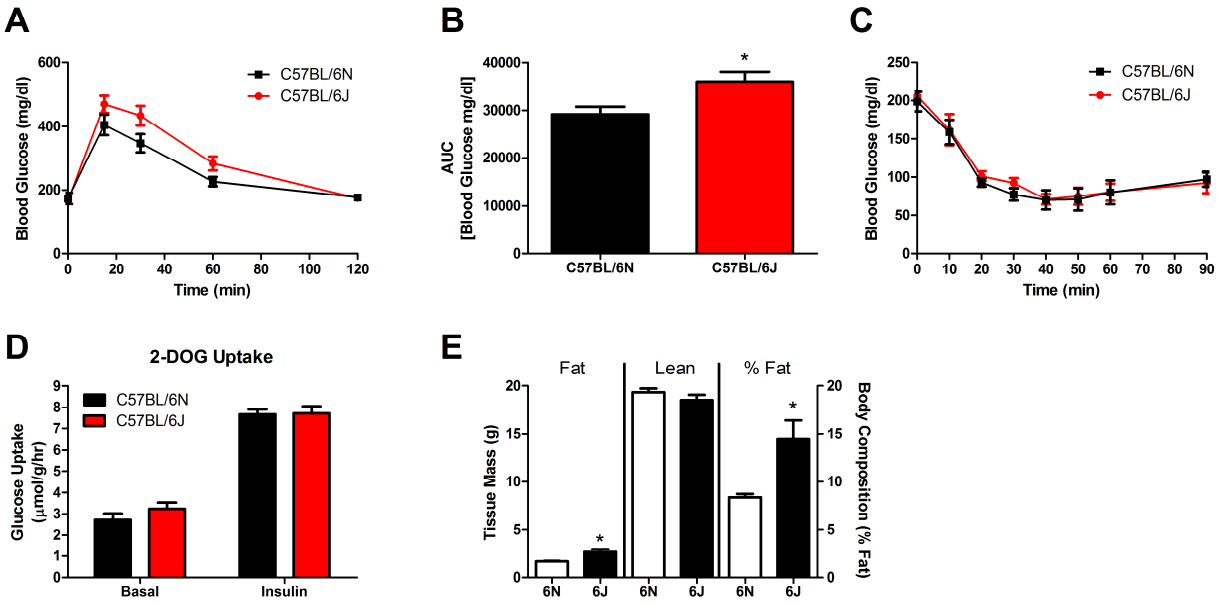

Figure 10. Reduced whole body O_2 consumption and energy expenditure in C57BL/6J mice, despite similar levels of activity and food intake. Indirect metabolic calorimetry and ambulatory activity in C57BL/6N and C57BL/6J mice. (**A**) Oxygen consumption and (**B**) Carbon dioxide production (**C**) calculated energy expenditure per gram of fat free mass. (**D**) Oxygen consumption (**E**) Carbon dioxide production and (**F**) calculated energy expenditure per gram of total body weight. (**G**) Calculated respiratory exchange ratio. (**H**) Food intake per 24 hour period. (**I**) Ambulatory activity. *Different from 6N mice within either the Light or Dark Cycle ($p < 0.05$). Data are mean ± SEM, n=13/group.

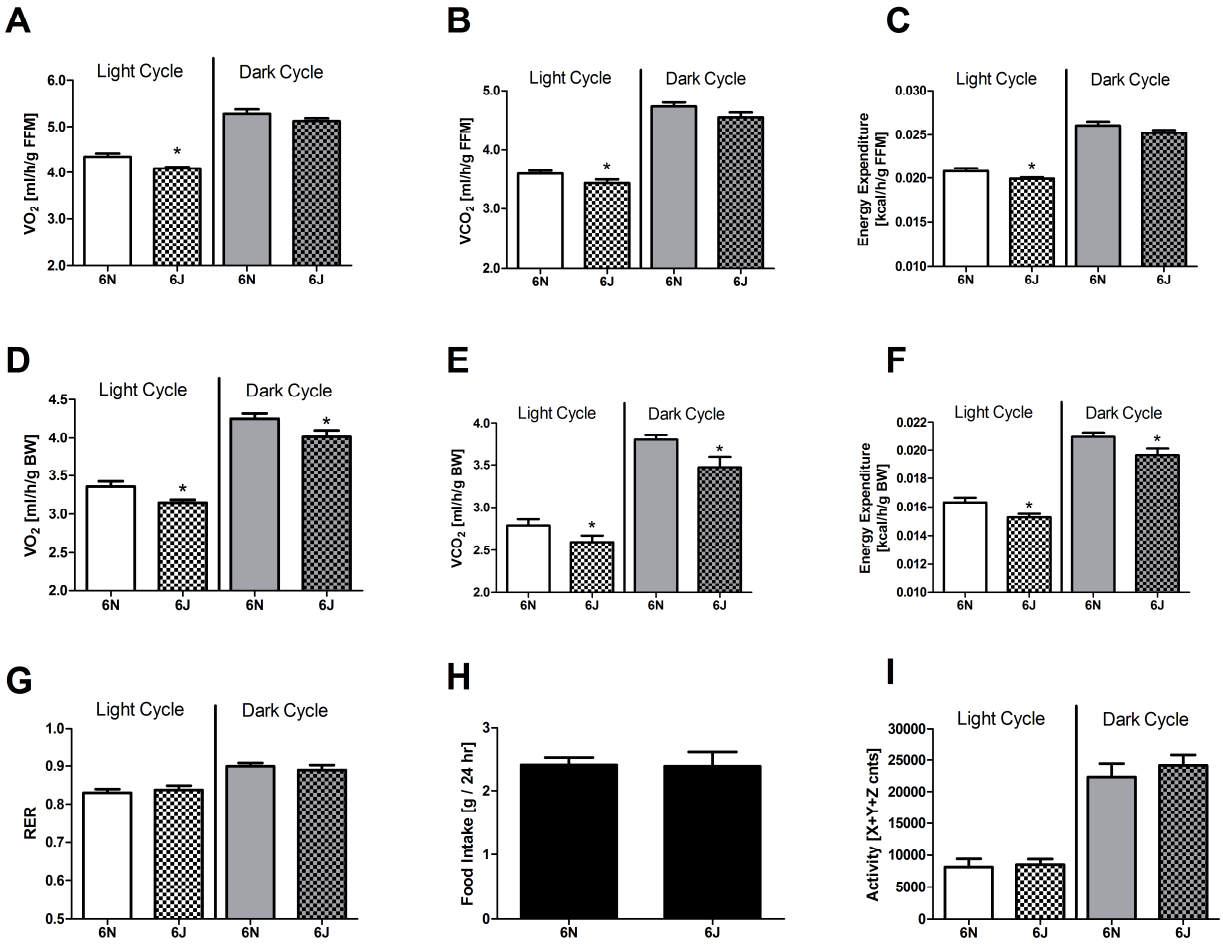

Figure 11. Markers of mitochondrial content are similar between C47BL/6N and C57BL/6J mice. (**A**) Western blot of mitochondrial complexes performed using homogenate prepared from frozen TA muscle. (**B**) Maximal uncoupled respiration was assessed in permeabilized fibers prepared from RG of C57BL/6N and C57BL/6J mice. Substrates included 10 mM glutamate, 2 mM malate, 2 mM ADP, 10 mM succinate, and 500 nM FCCP. Data are mean ± SEM, n=6-10/group.

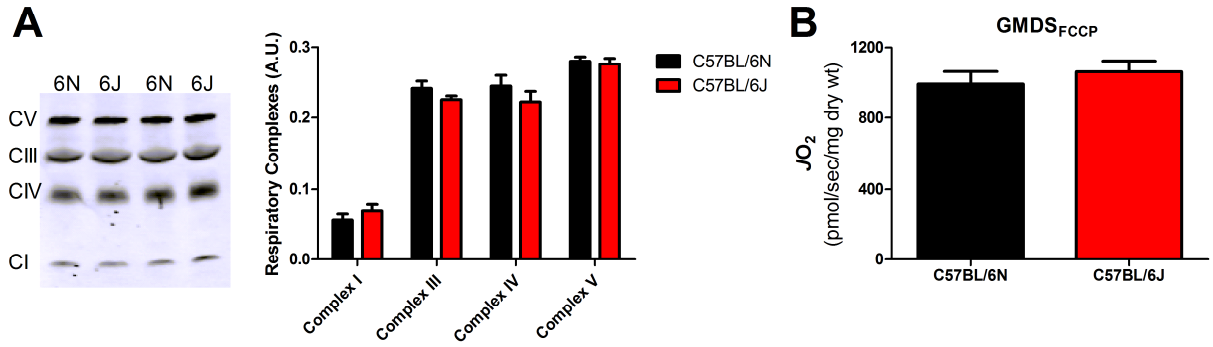

Figure 12. Differences in JO_2 consumption and mitochondrial membrane potential (ΔΨ) between C57BL/6N and C57BL/6J mice. (A-F) Permeabilized fibers were prepared from RG of C57BL/6N and C57BL/6J mice. (**A**) Oxygen consumption was assessed in response to 1 mM pyruvate, 5 mM carnitine and 2 mM ADP. *Different from C57BL/6N mice ($p < 0.05$). (**B**) Quantified ΔΨ in the presence of pyruvate/carnitine (1 mM/5 mM) under state 4 and state 3 (2 mM ADP) conditions. (**C**) Oxygen consumption was assessed in response to 1 mM pyruvate, 5 mM carnitine and 2 mM ADP in the absence (- DTT) or presence of 0.5 mM DTT (+ DTT). *Different from all other conditions ($p < 0.05$). (**D**) Representative experiment depicting the assessment of ΔΨ in the presence of pyruvate/carnitine (1 mM/5 mM). Trace reflects the voltage signal obtained in response a 5 point TPP^+ titration (1.1-1.5μM), following the addition of a permeabilized fiber and 2 mM ADP. (**E**) Oxygen consumption was assessed in response to 10 mM succinate. (**F**) Quantified ΔΨ in the presence of succinate (10 mM) under state 4 conditions. *Different from C57BL/6N mice ($p < 0.05$). Data are mean ± SEM, n=10-15/group.

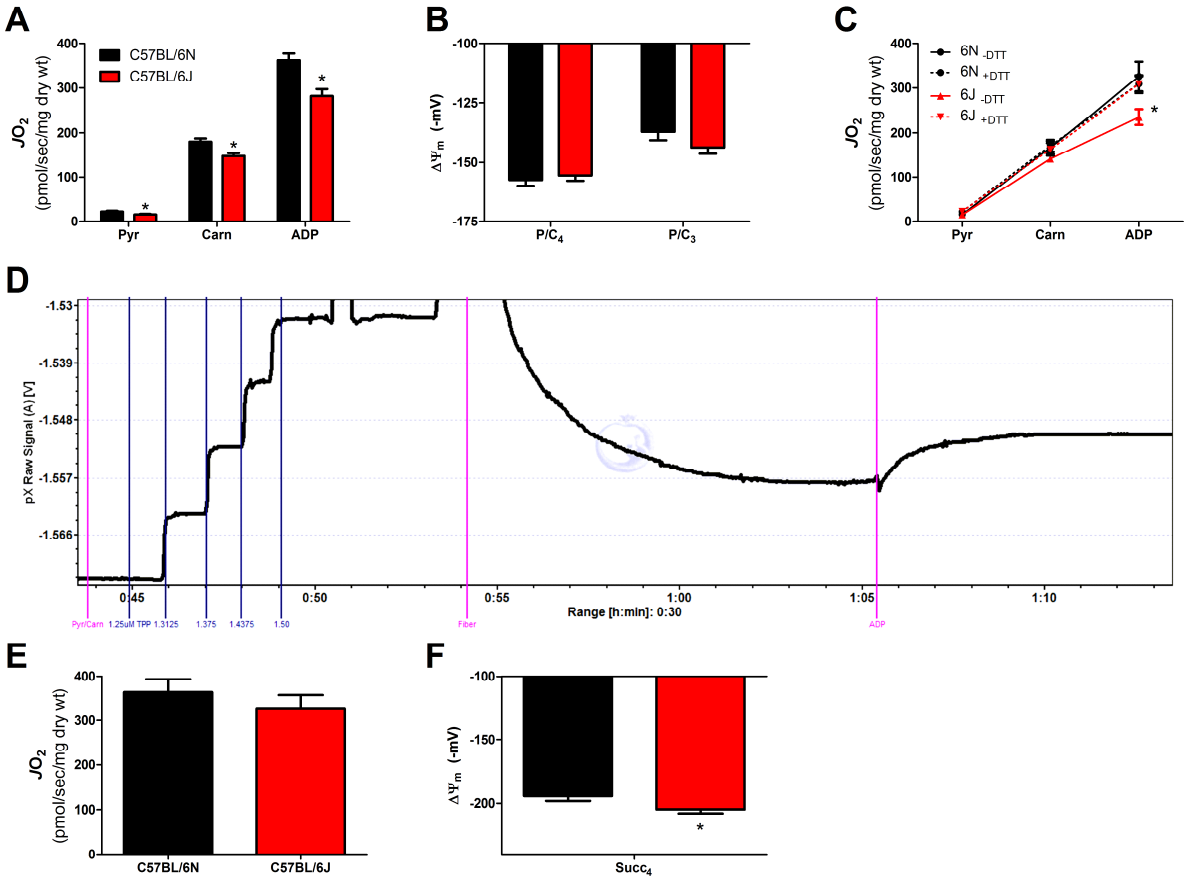

Figure 13. Pyruvate-supported JH_2O_2 emission is elevated in C57BL/6J mice. (A-H) Permeabilized fibers were prepared from RG of C57BL/6N and C57BL/6J mice. (**A**) JH_2O_2 emission in response to pyruvate (1 mM) alone. *Different from C57BL/6N ($p < 0.05$). (**B**) JH_2O_2 emission following the sequential addition of 1 mM pyruvate (Pyr) and 500 nM FCCP (Pyr_{FCCP}). *Different from C57BL/6N ($p < 0.05$). (**C**) Representative JH_2O_2 emission experiment following the sequential addition of 1 mM/5 mM pyruvate/carnitine (Pyr/Carn) and 100 μM/1 μM BCNU/auranofin (BCNU/AF). (**D**) Analyzed rates of JH_2O_2 emission from experiment depicted in panel C. *Different from C57BL/6N ($p < 0.05$); □ Different from Pyr/Carn rate in C57BL/6N mice ($p < 0.05$). (**E**) Representative JH_2O_2 emission experiment performed in C57BL/6N mice only following the sequential addition of 1 mM/5 mM pyruvate/carnitine (Pyr/Carn), 100 μM BCNU and 1 μM AF. (**F**) Analyzed rates of JH_2O_2 emission from experiment depicted in panel E. *Different from Pyr/Carn ($p < 0.05$); **Different from +BCNU ($p < 0.05$). (**G**) Representative JH_2O_2 emission experiment following the sequential addition of 1 mM/2 mM pyruvate/malate (Pyr/Mal) and 100 μM/1 μM BCNU/auranofin (BCNU/AF). (**H**) Analyzed rates of JH_2O_2 emission from experiment depicted in panel G. *Different from C57BL/6N ($p < 0.05$). Data are mean ± SEM, n=10-15/group.

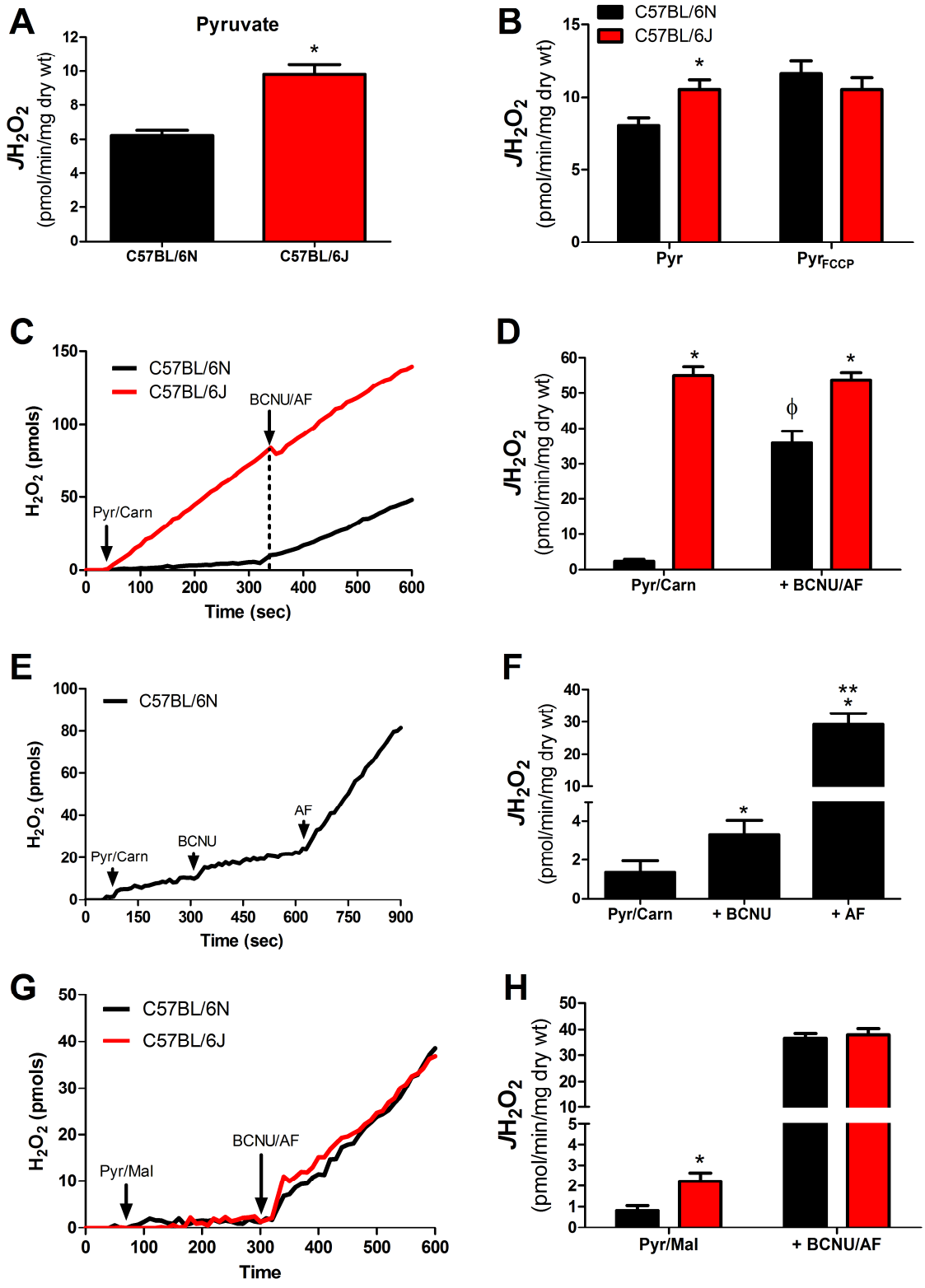
A
Pyruvate
JH_2O_2 (pmol/min/mg dry wt)
C57BL/6N
C57BL/6J
B
C57BL/6N
C57BL/6J
Pyr
Pyr_{FCCP}
C
C57BL/6N
C57BL/6J
BCNU/AF
Pyr/Carn
H_2O_2 (pmols)
Time (sec)
D
Pyr/Carn
+ BCNU/AF
E
C57BL/6N
Pyr/Carn
BCNU
AF
H_2O_2 (pmols)
Time (sec)
F
Pyr/Carn
+ BCNU
+ AF
G
C57BL/6N
C57BL/6J
Pyr/Mal
BCNU/AF
H_2O_2 (pmols)
Time
H
Pyr/Mal
+ BCNU/AF

Figure 14. Succinate-supported JH_2O_2 emission is elevated in C57BL/6J mice. **(A-C)** Permeabilized fibers were prepared from RG of C57BL/6N and C57BL/6J mice. (**A**) JH_2O_2 emission in response to succinate (10 mM) alone. *Different from C57BL/6N ($p < 0.05$). (**B**) Representative JH_2O_2 emission experiment following the sequential addition of 10 mM succinate and 100 µM/1 µM BCNU/auranofin (BCNU/AF). (**C**) Analyzed rates of JH_2O_2 emission from experiment depicted in panel B. *Different from C57BL/6N ($p < 0.05$); □ Different from corresponding – BCNU/AF rate ($p < 0.05$). Data are mean ± SEM, n=10-15/group.

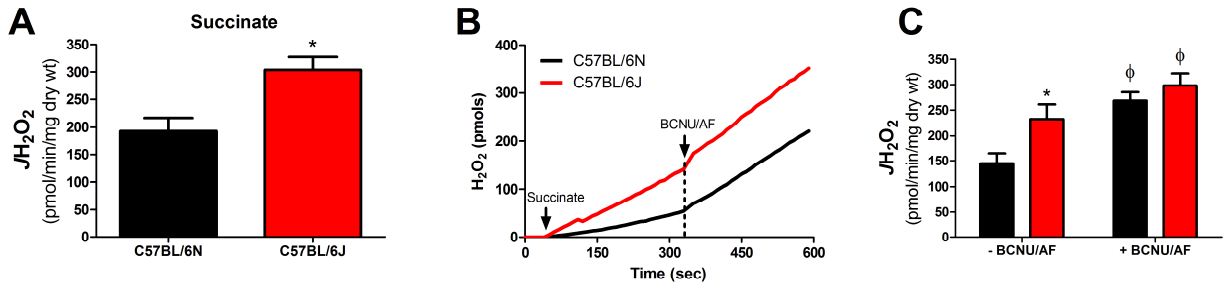

Figure 15. Glutathione redox status is unaltered in C57BL/6J mice. (**A-B**) Reduced (GSH) and oxidized (GSSG) glutathione, as well as the ratio of GSH/GSSG were assessed in homogenate prepared from frozen soleus (**A**) and TA (**B**) muscle.

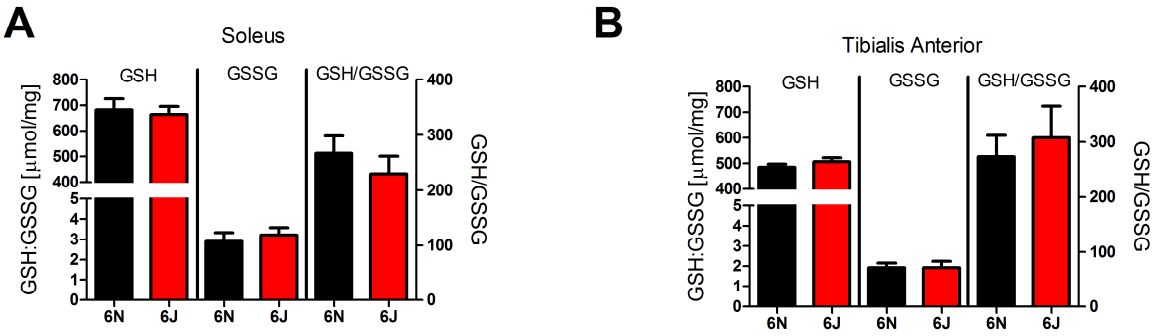

CHAPTER 4: INTEGRATED DISCUSSION

Major Findings

The production of H_2O_2 within biological systems was originally thought to exist merely as a deleterious byproduct of aerobic metabolism, that under normal (i.e., healthy) conditions were readily scavenged/degraded by the elaborate antioxidant defense machinery. At any one time point, the actual oxidative burden imposed to the system is dictated by the net balance of these two opposing systems (H_2O_2/ROS production vs. antioxidant buffering). In line with this notion, the term oxidative stress is commonly utilized as a general indication of any biological situation in which the production of H_2O_2 exceeds the ameliorating capabilities of the antioxidant defense system, potentially resulting in modification/ damage to various macromolecules (18). This definition vastly underestimates the complexity the cellular redox environment, as it has recently been demonstrated that the continual production of H_2O_2, at concentrations far below that indicative of “oxidative stress” is involved in the establishment of various redox signaling pathways, referred to as “redox circuits” (29). Disruptions in this signaling network either via increased peroxide production and/or decreased NADPH availability are likely the primary consequences of “oxidative stress”, rather than the more classical idea of radical-mediated damage to macromolecules (28). With respect to the continual source of H_2O_2 necessary for the establishment of redox circuitry, complex I and complex III within the ETS are commonly cited as the primary contributors in vivo (6, 52). Generation of H_2O_2 from these sites however is highly dependent on mitochondrial membrane potential, thus creating doubt as to whether H_2O_2 production would still be possible under conditions of high ATP demand (e.g.,

exercise). The matrix soluble dehydrogenases (53), as well as the ETF (49) are intriguing sources, as at least a portion of the H_2O_2 generate at these sites appears to be independent of membrane potential.

The results presented in Chapter II expand upon this work by demonstrating a role for PDH as a key H_2O_2-emitting site within skeletal muscle under physiological constraints (i.e., under ADP-stimulated conditions in the absence of respiratory inhibitors). PDH-derived H_2O_2 was found to be responsive to matrix nutrient balance (e.g., NADH/NAD^+) and redox buffering integrity, with the latter revealing a novel functional link between PDH and NNT (Figure 16). In Chapter III we investigated the impact of NNT loss, specifically within the C57BL/6J strain, on skeletal muscle mitochondrial respiratory kinetics and redox homeostasis, as well as whole body energy expenditure. Loss of functional NNT within the C57BL/6J mice was found to impair pyruvate-supported respiration, negatively shift mitochondrial membrane potential and dramatically increase H_2O_2 emitting potential within skeletal muscle mitochondria. With respect to the latter, we hypothesize that these findings may help to explain the increased susceptibility to HFD-induced insulin resistance previously demonstrated in the C57BL/6J mice, as elevations in mitochondrial H_2O_2 emitting potential has previously been linked to the development of diet-induced insulin resistance (2). While the effects observed specifically within skeletal muscle are certainly interesting, the consequences of NNT loss at the whole body level are perhaps more intriguing. Whole body O_2 consumption and energy expenditure were found to be decreased in C57BL/6J compared to C57BL/6N mice, despite no differences in RER, food intake or ambulatory activity. While the dependence of NNT-supported NADPH production is well known to

depend on the establishment of an electrochemical proton gradient across the inner mitochondrial membrane, this is the first evidence demonstrating a significant contribution of NNT-mediated Δp dissipation to resting energy expenditure. We hypothesize that these findings may help to explain the obesity prone-phenotype of the C57BL/6J mice demonstrated herein as well as by other investigators.

Future Directions

The present findings are novel in that they establish both PDH and NNT as principle regulators of the matrix redox environment specifically within skeletal muscle. The importance of the redox buffering network in regulating matrix redox status represents the potential for a paradigm shift within the field in which investigative focus begins to consider the impact of potential alterations in the activity of NADPH-producing enzymes to increasing overall peroxide burden during human disease. With respect to NNT, gain and loss of function experiments carried out in a tissue-specific manner will reveal much needed information related to the role of NNT in regulating redox homeostasis *in vivo*. To this end, methodological advances within the field of redox biochemistry which allow for *in vivo* assessment of H_2O_2 production and NADPH generation will be of paramount importance to deciphering the role of altered redox homeostasis in human disease.

Figure 16. PDH-derived JH_2O_2 production is a function of E2 reducing pressure and the matrix redox environment. The rate of H_2O_2 production from the PDH complex is principally determined by the redox status of the E2 bound lipoate residues,

which based on the ratio of DHLA/LA set the reducing pressure within the complex. E2 subunits are depicted as hexagons within the figure labeled “PDH Complex” with bound lipoate residues extending from 3 of the 6 faces. The redox pressure of a given E2 subunit is colorimetrically depicted and ranges from red (total oxidation) to blue (total reduction), based on the redox state of its exposed thiols. The gauge to right represents the average redox pressure within the complex and the corresponding rate of H_2O_2 production. H_2O_2 produced by the complex is buffered by the glutathione and thioredoxin redox systems, which derive NADPH from nicotinamide nucleotide transhydrogenase (NNT) in the presence of a functional electron transport system (ETS) and a NADH source. The NADH needed for this reaction could in theory arise from the PDH reaction, thus allowing for the complex to buffer its own H_2O_2. Panel **A** depicts the complex under low flux conditions (e.g., fasted state) in which pyruvate supply is minimal, redox pressure is low and antioxidant buffering capacity is high, thus resulting in low level H_2O_2 production and subsequent emission by the complex. Panel **B** illustrates the impact of accelerated pyruvate flux (e.g., fed state) and a reductive shift in E2 redox pressure, all of which places an increased demand on the redox buffering network and promotes accelerated production of H_2O_2 from PDH.

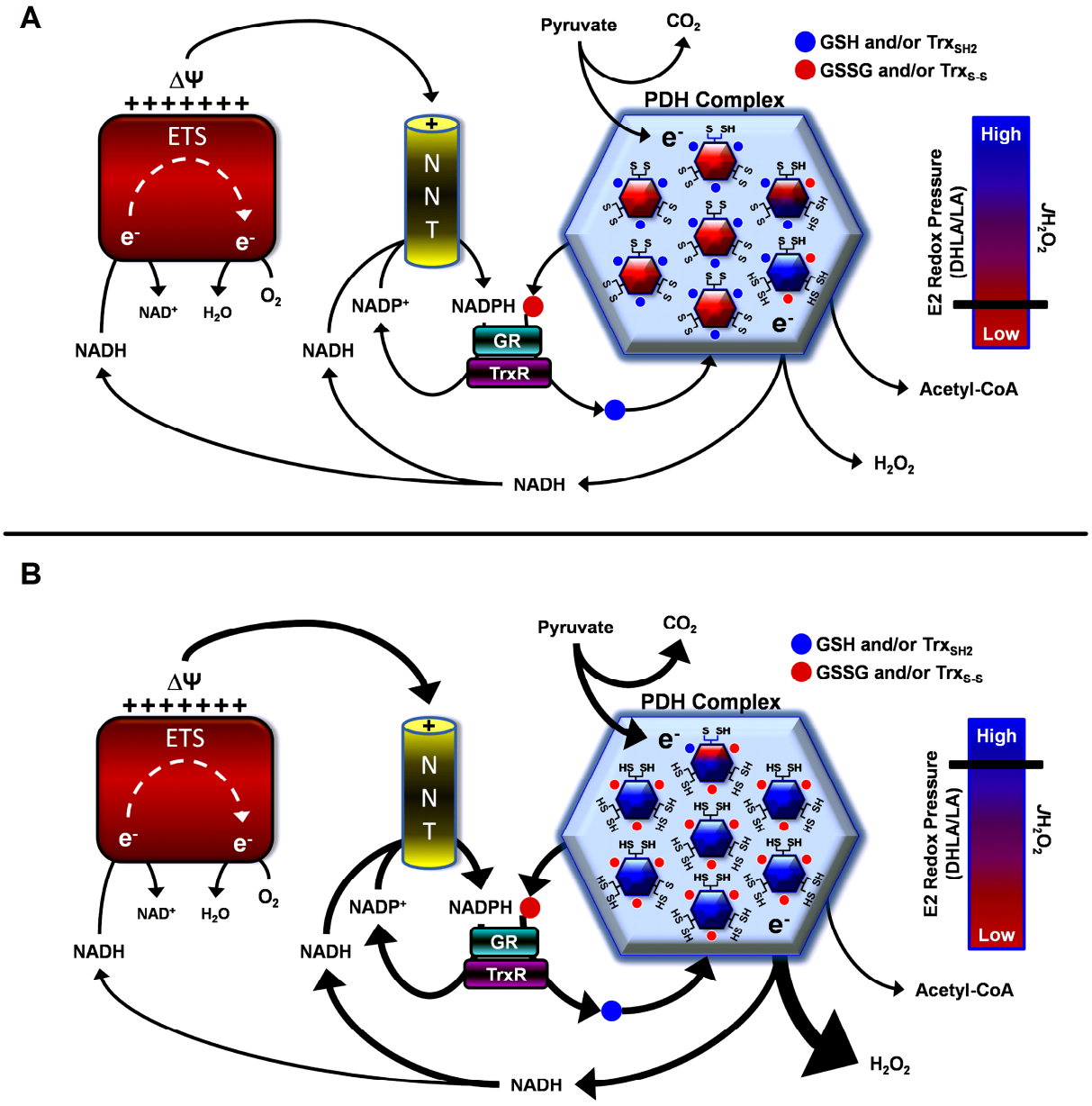
A
ΔΨ
+++++++
ETS
e-
e-
NAD+
H2O
O2
NADH
NNT
NADP+
NADPH
GR
TrxR
NADH
Pyruvate
CO2
PDH Complex
e-
e-
GSH and/or Trx SH2
GSSG and/or Trx S-S
E2 Redox Pressure (DHLA/LA)
High
Low
JH2O2
Acetyl-CoA
H2O2
NADH
B
ΔΨ
+++++++
ETS
e-
e-
NAD+
H2O
O2
NADH
NNT
NADP+
NADPH
GR
TrxR
NADH
Pyruvate
CO2
PDH Complex
e-
e-
GSH and/or Trx SH2
GSSG and/or Trx S-S
E2 Redox Pressure (DHLA/LA)
High
Low
JH2O2
Acetyl-CoA
H2O2
NADH

REFERENCES

1.**Adimora NJ, Jones DP, and Kemp ML**. A model of redox kinetics implicates the thiol proteome in cellular hydrogen peroxide responses. *Antioxid Redox Signal* 13: 731-743, 2010.

2.**Anderson EJ, Lustig ME, Boyle KE, Woodlief TL, Kane DA, Lin CT, Price JW, 3rd, Kang L, Rabinovitch PS, Szeto HH, Houmard JA, Cortright RN, Wasserman DH, and Neufer PD**. Mitochondrial H2O2 emission and cellular redox state link excess fat intake to insulin resistance in both rodents and humans. *The Journal of clinical investigation* 2009.

3.**Anderson EJ, and Neufer PD**. Type II skeletal myofibers possess unique properties that potentiate mitochondrial H(2)O(2) generation. *Am J Physiol Cell Physiol* 290: C844-851, 2006.

4.**Applegate MA, Humphries KM, and Szweda LI**. Reversible inhibition of alpha-ketoglutarate dehydrogenase by hydrogen peroxide: glutathionylation and protection of lipoic acid. *Biochemistry* 47: 473-478, 2008.

5.**Arkblad EL, Tuck S, Pestov NB, Dmitriev RI, Kostina MB, Stenvall J, Tranberg M, and Rydstrom J**. A Caenorhabditis elegans mutant lacking functional nicotinamide nucleotide transhydrogenase displays increased sensitivity to oxidative stress. *Free radical biology & medicine* 38: 1518-1525, 2005.

6.**Brand MD**. The sites and topology of mitochondrial superoxide production. *Exp Gerontol* 45: 466-472, 2010.

7.**Brautigam CA, Wynn RM, Chuang JL, and Chuang DT**. Subunit and catalytic component stoichiometries of an in vitro reconstituted human pyruvate dehydrogenase complex. *J Biol Chem* 284: 13086-13098, 2009.

8.**Bunik VI**. 2-Oxo acid dehydrogenase complexes in redox regulation. *Eur J Biochem* 270: 1036-1042, 2003.

9.**Bunik VI, and Sievers C**. Inactivation of the 2-oxo acid dehydrogenase complexes upon generation of intrinsic radical species. *Eur J Biochem* 269: 5004-5015, 2002.

10.**Chen CA, Wang TY, Varadharaj S, Reyes LA, Hemann C, Talukder MA, Chen YR, Druhan LJ, and Zweier JL**. S-glutathionylation uncouples eNOS and regulates its cellular and vascular function. *Nature* 468: 1115-1118, 2010.

11.**Chen L, Na R, Gu M, Salmon AB, Liu Y, Liang H, Qi W, Van Remmen H, Richardson A, and Ran Q**. Reduction of mitochondrial H2O2 by overexpressing peroxiredoxin 3 improves glucose tolerance in mice. *Aging cell* 7: 866-878, 2008.

12.**Dalle-Donne I, Rossi R, Colombo R, Giustarini D, and Milzani A**. Biomarkers of oxidative damage in human disease. *Clinical chemistry* 52: 601-623, 2006.

13.**Fisher-Wellman KH, and Neufer PD**. Linking mitochondrial bioenergetics to insulin resistance via redox biology. *Trends Endocrinol Metab* 23: 142-153, 2012.

14.**Forman HJ, Maiorino M, and Ursini F**. Signaling Functions of Reactive Oxygen Species. *Biochemistry* 49: 835-842, 2010.

15.**Freeman H, Shimomura K, Horner E, Cox RD, and Ashcroft FM**. Nicotinamide nucleotide transhydrogenase: a key role in insulin secretion. *Cell metabolism* 3: 35-45, 2006.

16.**Freeman HC, Hugill A, Dear NT, Ashcroft FM, and Cox RD**. Deletion of nicotinamide nucleotide transhydrogenase: a new quantitive trait locus accounting for glucose intolerance in C57BL/6J mice. *Diabetes* 55: 2153-2156, 2006.

17.**Go YM, Duong DM, Peng J, and Jones DP**. Protein Cysteines Map to Functional Networks According to Steady-state Level of Oxidation. *Journal of proteomics & bioinformatics* 4: 196-209, 2011.

18.**Halliwell B**. Reactive oxygen species in living systems: source, biochemistry, and role in human disease. *The American Journal of Medicine* 91: 14S-22S, 1991.

19.**Han D, Canali R, Rettori D, and Kaplowitz N**. Effect of glutathione depletion on sites and topology of superoxide and hydrogen peroxide production in mitochondria. *Mol Pharmacol* 64: 1136-1144, 2003.

20.**Hoehn KL, Salmon AB, Hohnen-Behrens C, Turner N, Hoy AJ, Maghzal GJ, Stocker R, Van Remmen H, Kraegen EW, Cooney GJ, Richardson AR, and James**

DE. Insulin resistance is a cellular antioxidant defense mechanism. *Proc Natl Acad Sci U S A* 106: 17787-17792, 2009.

21.**Hoek JB, and Rydstrom J**. Physiological roles of nicotinamide nucleotide transhydrogenase. *The Biochemical journal* 254: 1-10, 1988.

22.**Houstis N, Rosen ED, and Lander ES**. Reactive oxygen species have a causal role in multiple forms of insulin resistance. *Nature* 440: 944-948, 2006.

23.**Huang TT, Naeemuddin M, Elchuri S, Yamaguchi M, Kozy HM, Carlson EJ, and Epstein CJ**. Genetic modifiers of the phenotype of mice deficient in mitochondrial superoxide dismutase. *Human molecular genetics* 15: 1187-1194, 2006.

24.**Jackman MR, and Willis WT**. Characteristics of mitochondria isolated from type I and type IIb skeletal muscle. *Am J Physiol* 270: C673-678, 1996.

25.**Jackson JB, Peake SJ, and White SA**. Structure and mechanism of proton-translocating transhydrogenase. *FEBS Lett* 464: 1-8, 1999.

26.**Jeoung NH, and Harris RA**. Role of pyruvate dehydrogenase kinase 4 in regulation of blood glucose levels. *Korean Diabetes J* 34: 274-283, 2010.

27.**Jeoung NH, Wu P, Joshi MA, Jaskiewicz J, Bock CB, Depaoli-Roach AA, and Harris RA**. Role of pyruvate dehydrogenase kinase isoenzyme 4 (PDHK4) in glucose homoeostasis during starvation. *Biochem J* 397: 417-425, 2006.

28.**Jones DP**. Radical-free biology of oxidative stress. *Am J Physiol Cell Physiol* 295: C849-868, 2008.

29.**Jones DP, and Go YM**. Mapping the cysteine proteome: analysis of redox-sensing thiols. *Curr Opin Chem Biol* 2010.

30.**Kaku K, Fiedorek FT, Jr., Province M, and Permutt MA**. Genetic analysis of glucose tolerance in inbred mouse strains. Evidence for polygenic control. *Diabetes* 37: 707-713, 1988.

31.**Kang PT, Zhang L, Chen CL, Chen J, Green KB, and Chen YR**. Protein thiyl radical mediates S-glutathionylation of complex I. *Free Radic Biol Med* 53: 962-973, 2012.

32.**Kelley EE, Khoo NK, Hundley NJ, Malik UZ, Freeman BA, and Tarpey MM**. Hydrogen peroxide is the major oxidant product of xanthine oxidase. *Free radical biology & medicine* 48: 493-498, 2010.

33.**Kemp M, Go YM, and Jones DP**. Nonequilibrium thermodynamics of thiol/disulfide redox systems: a perspective on redox systems biology. *Free Radic Biol Med* 44: 921-937, 2008.

34.**Korshunov SS, Skulachev VP, and Starkov AA**. High protonic potential actuates a mechanism of production of reactive oxygen species in mitochondria. *FEBS Lett* 416: 15-18, 1997.

35.**Labajova A, Vojtiskova A, Krivakova P, Kofranek J, Drahota Z, and Houstek J**. Evaluation of mitochondrial membrane potential using a computerized device with a tetraphenylphosphonium-selective electrode. *Anal Biochem* 353: 37-42, 2006.

36.**Leto TL, Morand S, Hurt D, and Ueyama T**. Targeting and regulation of reactive oxygen species generation by Nox family NADPH oxidases. *Antioxid Redox Signal* 11: 2607-2619, 2009.

37.**Liu SS**. Cooperation of a "reactive oxygen cycle" with the Q cycle and the proton cycle in the respiratory chain--superoxide generating and cycling mechanisms in mitochondria. *J Bioenerg Biomembr* 31: 367-376, 1999.

38.**Liu SS**. Generating, partitioning, targeting and functioning of superoxide in mitochondria. *Biosci Rep* 17: 259-272, 1997.

39.**Mitchell P**. Coupling of phosphorylation to electron and hydrogen transfer by a chemi-osmotic type of mechanism. *Nature* 191: 144-148, 1961.

40.**Muoio DM, Noland RC, Kovalik JP, Seiler SE, Davies MN, DeBalsi KL, Ilkayeva OR, Stevens RD, Kheterpal I, Zhang J, Covington JD, Bajpeyi S, Ravussin E, Kraus W, Koves TR, and Mynatt RL**. Muscle-specific deletion of carnitine acetyltransferase compromises glucose tolerance and metabolic flexibility. *Cell metabolism* 15: 764-777, 2012.

41.**Nicholson A, Reifsnyder PC, Malcolm RD, Lucas CA, MacGregor GR, Zhang W, and Leiter EH**. Diet-induced obesity in two C57BL/6 substrains with intact or mutant nicotinamide nucleotide transhydrogenase (Nnt) gene. *Obesity (Silver Spring)* 18: 1902-1905, 2010.

42.**Ogata T, and Yamasaki Y**. Scanning electron-microscopic studies on the three-dimensional structure of mitochondria in the mammalian red, white and intermediate muscle fibers. *Cell Tissue Res* 241: 251-256, 1985.

43.**Pedersen A, Karlsson GB, and Rydstrom J**. Proton-translocating transhydrogenase: an update of unsolved and controversial issues. *J Bioenerg Biomembr* 40: 463-473, 2008.

44.**Perry CG, Kane DA, Lin CT, Kozy R, Cathey BL, Lark DS, Kane CL, Brophy PM, Gavin TP, Anderson EJ, and Neufer PD**. Inhibiting myosin-ATPase reveals a dynamic range of mitochondrial respiratory control in skeletal muscle. *Biochem J* 437: 215-222, 2011.

45.**Quinlan CL, Orr AL, Perevoshchikova IV, Treberg JR, Ackrell BA, and Brand MD**. Mitochondrial complex II can generate reactive oxygen species at high rates in both the forward and reverse reactions. *The Journal of biological chemistry* 287: 27255-27264, 2012.

46.**Rydstrom J**. Mitochondrial transhydrogenase--a key enzyme in insulin secretion and, potentially, diabetes. *Trends Biochem Sci* 31: 355-358, 2006.

47.**Sauer U, Canonaco F, Heri S, Perrenoud A, and Fischer E**. The soluble and membrane-bound transhydrogenases UdhA and PntAB have divergent functions in NADPH metabolism of Escherichia coli. *The Journal of biological chemistry* 279: 6613-6619, 2004.

48.**Schafer FQ, and Buettner GR**. Redox environment of the cell as viewed through the redox state of the glutathione disulfide/glutathione couple. *Free radical biology & medicine* 30: 1191-1212, 2001.

49.**Seifert EL, Estey C, Xuan JY, and Harper ME**. Electron transport chain-dependent and -independent mechanisms of mitochondrial H2O2 emission during long-chain fatty acid oxidation. *J Biol Chem* 285: 5748-5758, 2010.

50.**Sekhar RV, McKay SV, Patel SG, Guthikonda AP, Reddy VT, Balasubramanyam A, and Jahoor F**. Glutathione synthesis is diminished in patients with uncontrolled diabetes and restored by dietary supplementation with cysteine and glycine. *Diabetes care* 34: 162-167, 2011.

51.**Sekhar RV, Patel SG, Guthikonda AP, Reid M, Balasubramanyam A, Taffet GE, and Jahoor F**. Deficient synthesis of glutathione underlies oxidative stress in aging and can be corrected by dietary cysteine and glycine supplementation. *The American journal of clinical nutrition* 94: 847-853, 2011.

52.**St-Pierre J, Buckingham JA, Roebuck SJ, and Brand MD**. Topology of superoxide production from different sites in the mitochondrial electron transport chain. *The Journal of biological chemistry* 277: 44784-44790, 2002.

53.**Starkov AA, Fiskum G, Chinopoulos C, Lorenzo BJ, Browne SE, Patel MS, and Beal MF**. Mitochondrial alpha-ketoglutarate dehydrogenase complex generates reactive oxygen species. *J Neurosci* 24: 7779-7788, 2004.

54.**Surwit RS, Feinglos MN, Rodin J, Sutherland A, Petro AE, Opara EC, Kuhn CM, and Rebuffe-Scrive M**. Differential effects of fat and sucrose on the development of obesity and diabetes in C57BL/6J and A/J mice. *Metabolism: clinical and experimental* 44: 645-651, 1995.

55.**Surwit RS, Kuhn CM, Cochrane C, McCubbin JA, and Feinglos MN**. Diet-induced type II diabetes in C57BL/6J mice. *Diabetes* 37: 1163-1167, 1988.

56.**Surwit RS, Seldin MF, Kuhn CM, Cochrane C, and Feinglos MN**. Control of expression of insulin resistance and hyperglycemia by different genetic factors in diabetic C57BL/6J mice. *Diabetes* 40: 82-87, 1991.

57.**Toye AA, Lippiat JD, Proks P, Shimomura K, Bentley L, Hugill A, Mijat V, Goldsworthy M, Moir L, Haynes A, Quarterman J, Freeman HC, Ashcroft FM, and Cox RD**. A genetic and physiological study of impaired glucose homeostasis control in C57BL/6J mice. *Diabetologia* 48: 675-686, 2005.

58.**Treberg JR, Quinlan CL, and Brand MD**. Hydrogen peroxide efflux from muscle mitochondria underestimates matrix superoxide production--a correction using glutathione depletion. *FEBS J* 277: 2766-2778, 2010.

59.**Valko M, Leibfritz D, Moncol J, Cronin MT, Mazur M, and Telser J**. Free radicals and antioxidants in normal physiological functions and human disease. *The international journal of biochemistry & cell biology* 39: 44-84, 2007.

60.**Yin F, Sancheti H, and Cadenas E**. Silencing of nicotinamide nucleotide transhydrogenase impairs cellular redox homeostasis and energy metabolism in PC12 cells. *Biochimica et biophysica acta* 1817: 401-409, 2012.

61.**Zhang H, Go YM, and Jones DP**. Mitochondrial thioredoxin-2/peroxiredoxin-3 system functions in parallel with mitochondrial GSH system in protection against oxidative stress. *Arch Biochem Biophys* 465: 119-126, 2007.

62.**Zurlo F, Larson K, Bogardus C, and Ravussin E**. Skeletal muscle metabolism is a major determinant of resting energy expenditure. *The Journal of clinical investigation* 86: 1423-1427, 1990.

Appendix A: Animal Care and Use Protocol Approvals

East Carolina University

Animal Care and Use Commitee
212 Ed Warren Life Sciences Building
East Carolina University
Greenville, NC 27834

252-744-2436 office
252-744-2355 fax

November 19, 2012

Darrell Neufer, Ph.D.
Department of Physiology
Brody 6N-98
ECU Brody School of Medicine

Dear Dr. Neufer:

Your Animal Use Protocol entitled, "Breeding of Mice for Mitochondrial Bioenergetics and Metabolic Disease Studies" (AUP #Q285a) was reviewed by this institution's Animal Care and Use Committee on 11/19/12. The following action was taken by the Committee:

"Approved as submitted"

Please contact Dale Aycock at 744-2997 prior to hazard use

A copy is enclosed for your laboratory files. Please be reminded that all animal procedures must be conducted as described in the approved Animal Use Protocol. Modifications of these procedures cannot be performed without prior approval of the ACUC. The Animal Welfare Act and Public Health Service Guidelines require the ACUC to suspend activities not in accordance with approved procedures and report such activities to the responsible University Official (Vice Chancellor for Health Sciences or Vice Chancellor for Academic Affairs) and appropriate federal Agencies.

Sincerely yours,

Susan McRae, Ph.D.
Chair, Animal Care and Use Committee

SM/jd

enclosure

East Carolina University

Animal Care and
Use Commitee
212 Ed Warren Life
Sciences Building
East Carolina University
Greenville, NC 27834

252-744-2436 office
252-744-2355 fax

November 26, 2012

Darrell Neufer, Ph.D.
Department of Physiology
Brody 6N-98
ECU Brody School of Medicine

Dear Dr. Neufer:

Your Animal Use Protocol entitled, "Mitochondrial Bioenergetics and Metabolic Disease - Rat" (AUP #Q238b) was reviewed by this institution's Animal Care and Use Committee on 11/26/12. The following action was taken by the Committee:

"Approved as submitted"

Please contact Dale Aycock at 744-2997 prior to hazard use

A copy is enclosed for your laboratory files. Please be reminded that all animal procedures must be conducted as described in the approved Animal Use Protocol. Modifications of these procedures cannot be performed without prior approval of the ACUC. The Animal Welfare Act and Public Health Service Guidelines require the ACUC to suspend activities not in accordance with approved procedures and report such activities to the responsible University Official (Vice Chancellor for Health Sciences or Vice Chancellor for Academic Affairs) and appropriate federal Agencies.

Sincerely yours,

Susan McRae, Ph.D.
Chair, Animal Care and Use Committee

SM/jd

enclosure

East Carolina University

Animal Care and
Use Commitee
212 Ed Warren Life
Sciences Building
East Carolina University
Greenville, NC 27834

252-744-2436 office
252-744-2355 fax

November 26, 2012

Darrell Neufer, Ph.D.
Department of Physiology
Brody 6N-98
ECU Brody School of Medicine

Dear Dr. Neufer:

Your Animal Use Protocol entitled, "Mitochondrial Bioenergetics and Metabolic Disease - Mice" (AUP #Q237b) was reviewed by this institution's Animal Care and Use Committee on 11/26/12. The following action was taken by the Committee:

"Approved as submitted"

Please contact Dale Aycock at 744-2997 prior to hazard use

A copy is enclosed for your laboratory files. Please be reminded that all animal procedures must be conducted as described in the approved Animal Use Protocol. Modifications of these procedures cannot be performed without prior approval of the ACUC. The Animal Welfare Act and Public Health Service Guidelines require the ACUC to suspend activities not in accordance with approved procedures and report such activities to the responsible University Official (Vice Chancellor for Health Sciences or Vice Chancellor for Academic Affairs) and appropriate federal Agencies.

Sincerely yours,

Susan McRae, Ph.D.
Chair, Animal Care and Use Committee

SM/jd

enclosure

Appendix B: Institutional Review Board Use & Care of Human Subjects Approval

EAST CAROLINA UNIVERSITY
University & Medical Center Institutional Review Board Office
1L-09 Brody Medical Sciences Building• 600 Moye Boulevard • Greenville, NC 27834
Office **252-744-2914** • Fax **252-744-2284** • **www.ecu.edu/irb**

TO: P. Darrell Neufer, PhD, Department of EXSS, ECU, Brody 6N-98

FROM: UMCIRB

DATE: December 7, 2010

RE: Full Committee Approval for Continuing Review of a Research Study Requiring Modifications

TITLE: Linking Mitochondrial Bioenergetics to Muscle Insulin Sensitivity

UMCIRB #08-0699

The above referenced research study was initially reviewed by the convened University and Medical Center Institutional Review Board (UMCIRB) on **11/26/08 & 12/10/08.** The research study underwent a subsequent continuing review for approval on 11/10/10 by the convened UMCIRB. Requested modifications were prescribed and received final approval on 12/7/10 by expedited review. The UMCIRB deemed this **NIH/NIDDK** sponsored study **more than minimal risk** requiring a continuing review in **12 months.** Changes to this approved research may not be initiated without UMCIRB review except when necessary to eliminate an apparent immediate hazard to the participant. All unanticipated problems involving risks to participants and others must be promptly reported to the UMCIRB. The investigator must submit a continuing review/closure application to the UMCIRB prior to the date of study expiration. The investigator must adhere to all reporting requirements for this study.

The above referenced research study has been given approval for the period of **11/10/10** to **11/9/11.** The approval includes the following items:

- Continuing Review Form (dated 10/15/10)
- Research protocol
- Protocol summary
- Informed consent: Muscle Biopsy and IVGTT (dated 12/14/09)
- Informed consent: Mito Restoration (dated 12/14/09)
- Informed consent: Acute High Fat Study in Leans (dated 12/14/09)
- Informed consent: Acute High Carbohydrate Study in Leans (dated 12/14/09)
- Informed consent: Chronic High Fat Study in Leans (dated 12/14/09)
- Informed consent: Exercise in Obese (dated 12/14/09)
- Informed consent: High Fat Diet and Exercise in Leans (12/14/09)
- International physical activity questionnaire (dated 8/02)
- 3-day diet record guidelines
- STRRIDE 3-day diet record
- Personal history form
- Flyer

The following UMCIRB members were recused for reasons of potential for Conflict of Interest on this research study:
R. Hickner

NOTE: The following UMCIRB members with a potential Conflict of Interest did not attend this IRB meeting:
None

The UMCIRB applies 45 CFR 46, Subparts A-D, to all research reviewed by the UMCIRB regardless of the funding source. 21 CFR 50 and 21 CFR 56 are applied to all research studies under the Food and Drug Administration regulation. The UMCIRB follows applicable International Conference on Harmonisation Good Clinical Practice guidelines.